Geothermics 64 (2016) 163–179

Contents lists available at ScienceDirect

Geothermics

journal homepage: www.elsevier.com/locate/geothermics

Mechanical behaviour of the Rotokawa Andesites (New Zealand): Insight into permeability evolution and stress-induced behaviour in an actively utilised geothermal reservoir

P.A. Siratovich[a,*], M.J. Heap[b,*], M.C. Villeneuve[a], J.W. Cole[a], B.M. Kennedy[a], J. Davidson[a], T. Reuschlé[b]

[a] Department of Geological Sciences, University of Canterbury, Private Bag 4800, Christchurch 8140, New Zealand
[b] Géophysique Expérimentale, Institut de Physique de Globe de Strasbourg (UMR 7516 CNRS, Université de Strasbourg/EOST), 5 rue René Descartes, 67084 Strasbourg Cedex, France

ARTICLE INFO

Article history:
Received 16 March 2016
Received in revised form 16 May 2016
Accepted 24 May 2016

Keywords:
Permeability
Triaxial deformation
Geothermal
Rotokawa
Well stability
Seismicity

ABSTRACT

High-enthalpy geothermal systems, such as that of Rotokawa in the central Taupo Volcanic Zone (TVZ) of New Zealand, commonly host fracture systems that control reservoir permeability. The loss of porosity and permeability through compaction and mineral precipitation, and the opening of permeable fracture zones, occurred in tandem as the geothermal system evolved. In order to better understand how porosity can evolve in an active reservoir, a systematic study of triaxial deformation experiments has been undertaken to investigate the mechanical behaviour and failure mode of coherent andesite lavas and andesite breccias (the predominant reservoir lithologies) with varying porosity and alteration intensity from the Rotokawa Geothermal Field under high confining pressure and high pore fluid pressure conditions. These experiments provide insight into the formation of permeable fracture zones and low-permeability zones within the reservoir. Although we observed brittle failure mode in all our experiments (covering a range of rock attributes and relevant pressure conditions), we find that the amount of dilatancy during deformation, inferred to assist in the creation of a permeable network, is considerably reduced at high effective pressures and for high-porosity and highly altered samples. Importantly, some high-porosity and/or highly altered samples experienced a net compaction at the end of the experiments. Microstructural observations suggest that, although the failure mode remains ultimately brittle, microcracking and pore collapse can operate in concert at high effective pressure, porosity, and/or alteration, potentially explaining the reduction in dilatancy. We infer, therefore, that the deformation of the rocks within the reservoir could result in either a bulk permeability increase or a permeability decrease, depending on the physical characteristics of the rocks (e.g. porosity and alteration intensity) and the pressure conditions. Using our new experimental data we provide a Hoek-Brown failure criterion for an intact Rotokawa andesite with a representative porosity and show the distribution of stresses around a vertical and deviated borehole during drilling using a finite element model. Finite element modelling shows that brittle failure of intact rock (and therefore off-fault seismicity) during production and injection is unlikely in RKA containing the average porosity assumed for the reservoir. Production-induced compaction and injection-induced tensile failure could occur however in high-porosity and/or highly altered intact rock (which could lead to instability at the well boundary), particularly in deviated wells. The experiments and modelling presented herein provide insight into the evolution of an actively utilised geothermal reservoir.

© 2016 Elsevier Ltd. All rights reserved.

1. Introduction

Fractures are near-ubiquitous in crustal rocks and are known to reduce rock mass strength (Hoek and Brown, 1980), control stress (Townend and Zoback 2000), and greatly modify the permeability of the shallow crust (Brace 1980; Antonellini and Aydin, 1994; Barton et al., 1995; Caine et al., 1996; Rawling et al., 2001;

* Corresponding authors.
E-mail addresses: paul.siratovich@gmail.com (P.A. Siratovich), heap@unistra.fr (M.J. Heap).

http://dx.doi.org/10.1016/j.geothermics.2016.05.005
0375-6505/© 2016 Elsevier Ltd. All rights reserved.

Heap and Kennedy, 2016). Constraining the mechanical behaviour of rock under a differential stress is therefore of crucial importance to understanding the evolution of the permeability of a rock mass. This is especially important in the context of managing subsurface geological resources, such as those that contain hydrocarbons (Segall and Fitzgerald, 1998), geothermal fluids (Ghassemi, 2012), and the emerging field of carbon dioxide sequestration (Zoback and Gorelick, 2012). Geothermal reservoirs are one such environment that is particularly prone to large variations in temperature, stress, and pressure (pore fluid and lithostatic pressure) in both time and space (Grant and Bixley, 2011). The occurrences of geothermal resources are often associated with high fluid flow rates, large temperature perturbations, and significant crustal stresses (Bibby et al., 1995; Cole, 1990; Rowland and Sibson, 2004; Rowland et al., 2010). As a result, the hydraulic and mechanical behaviour of these subsurface systems, properties that are influenced by both pressure and temperature, are also subject to variations in time and space. In an actively utilised geothermal reservoir, understanding the response of the stress field during production and injection of reservoir fluids is important for assessing the longevity of a particular resource. Wellbore stability (Zoback, 2010), subsidence (Allis et al., 2009; Keiding et al., 2010), and seismicity (Ellsworth, 2013; Sewell et al., 2015; Sherburn et al., 2015) are some of the consequences of changing reservoir pressures due to production and injection. The destruction of porosity during deformation can be deleterious to geothermal reservoir productivity. Compactant deformation—promoted by high effective pressures (Wong and Baud, 2012) (defined here as simply the confining pressure minus the pore fluid pressure)—can be instigated by a reduction in reservoir rock pore pressure and potentially lead to borehole stability and surface subsidence issues. Conversely, the lengthening and widening of pre-existing cracks, and the formation of new cracks, during deformation can enhance the porosity and permeability of the system. For these and other reasons, detailed investigations in the laboratory that investigate the processes which may lead to such behaviour can provide a better understanding of the development of permeability in geothermal reservoirs and assist in planning for operations that may induce wellbore instability, subsidence, or destroy or enhance permeability.

The current understanding of mechanical behaviour of rocks under varying stress conditions is well established, but not exhaustive (e.g. Paterson and Wong, 2005; Wong and Baud, 2012). Research on this topic has focused primarily on the mechanical behaviour of siliciclastic rocks (e.g. Wong et al., 1997; Baud et al., 2006) and carbonate rocks (e.g. Baud et al., 2009; Vajdova et al., 2004, 2012), with particular emphasis on understanding the conditions that result in a brittle or ductile response to an applied differential stress. In studies of rock deformation in compression, material failure is often assigned as either brittle or ductile (e.g. Evans et al., 1990; Paterson and Wong, 2005), terms used to describe the mechanical behaviour and failure mode of an experimental sample. While brittle behaviour is synonymous with strain localisation (typically the coalescence of tensile microcracks to form a throughgoing axial split or shear fracture), ductile behaviour is defined as the capacity of a material to deform to substantial strain without the tendency to localise the flow into faults (Rutter, 1986). Therefore, while microcracking promotes brittle behaviour on the microscale, there are numerous micromechanisms that can promote ductility, including microcracking in the case of cataclastic flow (Menéndez et al., 1996). We note however that ductile behaviour can be associated with strain localisation, such as compaction bands, in specific circumstances (e.g. Baud et al., 2004, 2006; Heap et al., 2015a).

Experiments have shown that permeability evolution during deformation depends on the failure mode and the initial porosity of the rock. While ductile deformation leads to reductions in porosity and permeability (Zhu and Wong, 1997; Baud et al., 2012), permeability evolution in the brittle regime has been observed to increase and decrease permeability for low- (Mitchell and Faulkner, 2008) and high-porosity rocks (Zhu and Wong, 1997), respectively.

The mechanical response of volcanogenic rocks—rocks containing a much greater microstructural complexity than sandstone or limestone—to a differential stress, and the micromechanical processes that constrain the resultant behaviour, still requires further investigation. Triaxial deformation studies probing mechanical behaviour exist for andesite (Bauer et al., 1981; Loaiza et al., 2012; Heap et al., 2015b; Farquharson et al., 2016; Heap and Wadsworth, 2016), tuff (Zhu et al., 2011; Heap et al., 2015c), basalt (Bauer et al., 1981; Shimada, 1986; Violay et al., 2012; Adelinet et al., 2013; Violay et al., 2015), and dacite (Kennedy et al., 2009; Smith et al., 2011). These studies have highlighted that high- and low-porosity volcanic rocks are brittle at low effective pressures (i.e. shallow depths), whereas ductile behaviour, driven by cataclastic pore collapse on the microscale, can occur in porous volcanic rocks at high effective pressures (i.e. deep depths) (Shimada, 1986; Zhu et al., 2011; Loaiza et al., 2012; Adelinet et al., 2013; Heap et al., 2015b,c). A recent study (Heap et al., 2015b) highlighted that there is still much to learn regarding the mechanical behaviour of volcanic rocks, such as the influence of pore size and pore size distribution. In particular, there are very few triaxial data on (typically altered) volcanic rocks sourced directly from active geothermal resources (uniaxial data are available in Siratovich et al. (2014) and Wyering et al., (2014)). Studies focussed on the behaviour of altered geothermal rock during deformation will inform on permeability development, material competency, and reservoir evolution.

In this paper we present a new experimental dataset and investigation of one such geothermal reservoir rock that hosts a high-enthalpy geothermal system, the Rotokawa Andesite (RKA) (McNamara et al., 2016). Through a systematic investigation of core sourced from this important reservoir, we aim to address the following questions: (1) Under what stress conditions does the RKA behave in a brittle manner? Can the brittle-ductile transition be achieved in a laboratory setting, and if so, what are the implications for the natural reservoir state? (2) How does hydrothermal alteration influence the mechanical behaviour and failure mode of the RKA? (3) What are the micromechanical mechanisms that control the deformation of RKA under an applied stress field and what are the implications for seismicity, wellbore stability, and permeability development or destruction? (4) Is it possible for a natural or anthropogenic shift in the stress state to promote deformation that may have negative implications for reservoir permeability and wellbore stability?

To address these questions, we present new mechanical data from triaxial deformation experiments on RKA (that allow the measurement of sample porosity change during deformation) and modelling designed to study the likely performance of the RKA during production and injection.

2. Materials and experimental methods

2.1. Rotokawa Andesite (RKA)

The Rotokawa Geothermal Field is located in the central Taupo Volcanic Zone, North Island, New Zealand (Fig. 1 a). The field boasts two commercial power plants: Rotokawa I and Nga Awa Purua; these power plants generate approximately 34 and 140 MWe, respectively (McNamara et al., 2016). Production and injection (Fig. 1b) of the fluids utilised in these stations is hosted primarily within the Rotokawa Andesite (RKA). RKA is found at approximately 1500–2500 m below surface (Fig. 1c). Spot cores of RKA were obtained during the drilling of production wells RK27, RK27L2,

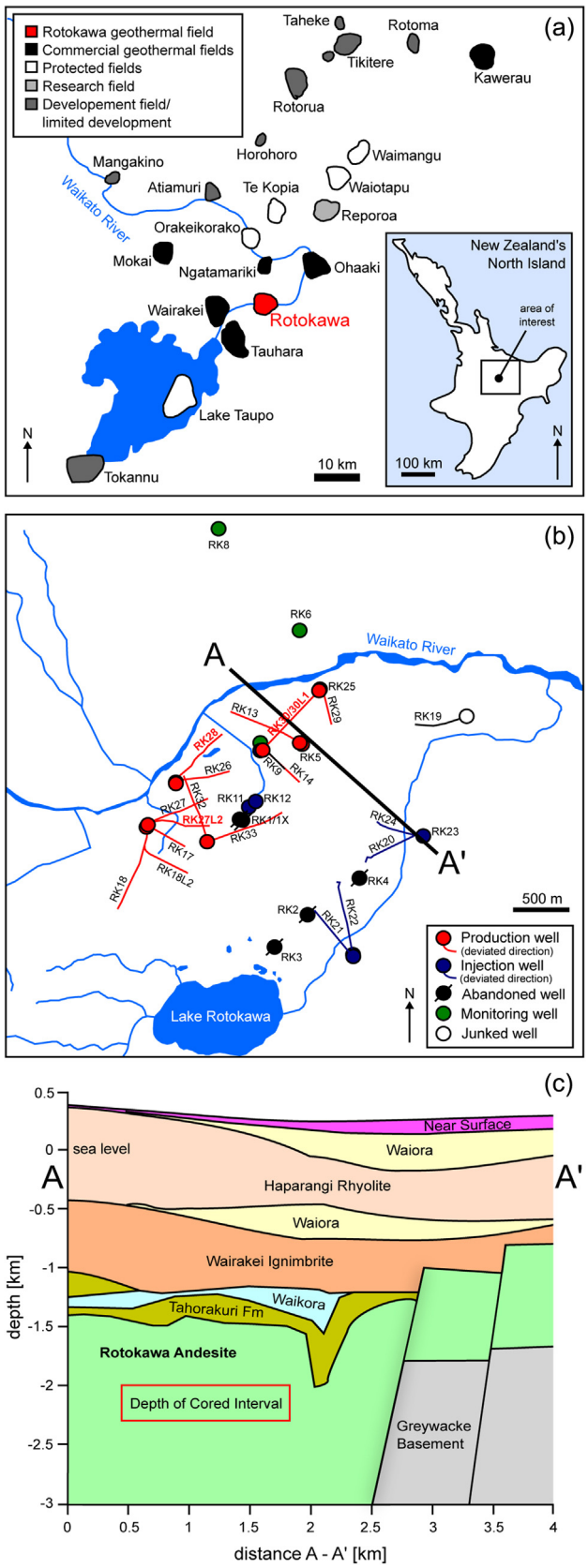

Fig. 1. (a) Geothermal systems of the Taupo Volcanic Zone (New Zealand). Location of the Rotokawa Geothermal Field shown in red. Inset shows a map of New Zealand's North Island. (b) Map of Rotokawa Geothermal Field showing the location and orientation of the main geothermal wells. Line A-A' is the line used for the cross section shown in panel (c). (c) Simplified cross section through Rotokawa Geothermal Field showing stratigraphic location of the Rotokawa Andesite and the depth of the cored interval. Panels (a) and (b) were taken from Siratovich et al. (2015b). Panel (c) is modified from Winick et al. (2011).

RK28, and RK29 (Siratovich et al., 2014) and are representative of the rock within the major feed zones of the geothermal reservoir. The andesite reservoir has *in-situ* temperatures as high as 340 °C (Winick et al., 2011) and reservoir pressures (pore pressures) on the order of 15–20 MPa (Quinao et al., 2013).

The geology of the RKA is complex (general descriptions of RKA are given in Browne et al. (1992) and Rae (2007)). The RKA consists of a series of calc-alkaline, medium-low potassium andesitic lavas and breccias that have experienced significant hydrothermal alteration from the high-enthalpy geothermal system (Figs. 2–4). The rocks of the RKA display a propylitic-style hydrothermal mineral assemblage (Rae, 2007). Primary mineralogy of the RKA is dominated by phenocrysts of plagioclase (0.5–4 mm in diameter) and pyroxene (<2 mm) hosted in a groundmass containing plagioclase, pyroxene, and titanomagnetite microlites. Plagioclase phenocrysts are partially resorbed and microcracked (as shown in the scanning electron microscope (SEM) photograph presented as Fig. 3a) with variable degrees of alteration/replacement to albite, adularia, occasional calcite, and rare pyrite. Pyroxene phenocrysts are partially to totally altered/replaced by chlorite, quartz, calcite, and epidote. The groundmass of these materials is generally strongly altered to chlorite and silica minerals, with titanomagnetite commonly replaced by leucoxene. The characteristics of the porosity vary between the samples (e.g. Table 1; Fig. 2a–d). Pores are irregularly shaped and some are filled with chlorite, quartz, epidote, and/or calcite (Fig. 3b). Pores also exist between fragments in the lava breccias, or within minerals dissolved by fluids (Fig. 3d), and some pores show evidence of collapse (Figs. 3e-f). Fractures are present both within and across individual fragments or phenocrysts (inter- or *trans*-granular) and can be lined or infilled with epidote, chlorite, and/or calcite.

The samples of RKA tested in this study are from drill core from depths between 1850 and 2315 m (Table 1). The core samples show extreme differences in macro-texture, both in the amount of brecciation and the degree of alteration (Fig. 4), even within a small vertical distance within the core (e.g. sample 28.14.2 (Fig. 4c) is a lava with only moderate alteration, while 28.14.7 (Fig. 4a), from almost the same depth, is a strongly altered breccia containing veins (largely of epidote and quartz) between angular fragments of intensely altered andesite). Veins of altered andesitic clasts in a finer groundmass crosscut some lava samples (e.g. Fig. 4b).

2.2. Sample preparation and experimental methods

Sections of the intact (i.e. pre-deformation in the laboratory) original core obtained during development drilling (100 mm diameter) were over-cored to obtain cylindrical samples 20 mm in diameter and nominally 40 mm in length. The samples were washed then dried in a vacuum oven at 40 °C and near −1.0 bar gauge vacuum. The dried cores were then weighed and vacuum saturated with distilled water. After saturation, water-wet and Archimedes weights were measured. These values were then used in the calculation of porosity and bulk density of the samples following the method reported in Guéguen and Palciauskas (1994). Porosity will be presented as a fraction (e.g. $\Phi = 15\% = 0.150$) to make changes in porosity easier to communicate.

After porosity determination, each water-saturated sample was jacketed in a nitrile sleeve and capped with a solid steel endcap on the top of the sample and a steel pore fluid distribution plate on the bottom of the sample. The sample was then placed into the triaxial deformation apparatus at the Université de Strasbourg (Fig. 5) and the apparatus was closed. Confining pressure (kerosene) was

Table 1
Descriptions of the samples used in this study. R = rare; M = moderate; C = common.

Alteration type	Sample number	Depth (m)	Pores	Connected Porosity	Veins	Comments
Moderately altered andesite lava/breccia	27L2.3.7a	2123	C	0.102	None	Highly porphyritic; irregular pores lined with silica minerals (Fig. 2a and b)
	27L2.21.2b	2121	M/R	0.125	None	Sample has brecciated andesite vein through lava
	27.TJ11 (samples 1 and 4)	1852	M	0.151(range 0.148–0.153)	None	Clasts in matrix. Less porphyritic; pores small and rounded (Fig. 2g and h)
	28.10.5b	2310	C	0.080	R	(as above) (Fig. 2c and 2d)
	28.11.1b2	2311	M	0.068	None	(as above)
	28.14.2 (samples 1–5)	2314	M	0.096 (range 0.095–0.098)	None	(as above)
	28.11.3a	2311	M	0.093	None	Some quartz and calcite in pores
Highly altered andesite lava/breccia	29.TJ14 (samples 2 and 4)	2081	M	0.178	R	Lava. Phenocrysts totally altered (see Fig. 2i and j)
	28.14.5	2314	M	0.140	C	Angular breccia. Phenocrysts totally altered; veins largely of epidote/calcite (Figs. 2e and 2f)

Table 2
Summary of the triaxial testing on samples from a single core of RKA. P_c = confining pressure; P_p = pore fluid pressure; P_{eff} = effective pressure.

Sample	Connected Porosity	P_c (MPa)	P_p (MPa)	P_{eff} (MPa)	Effective mean stress P at the peak stress (MPa)	Differential stress Q at the peak stress (MPa)	Failure Mode
28.14.2.6	0.097	75	70	5	47	124	Shear Fracture
28.14.2.4	0.095	75	45	30	98	205	Shear Fracture
28.14.2.5	0.097	75	25	50	129	236	Shear Fracture
28.14.2.1	0.098	75	5	70	154	253	Shear Fracture
28.14.2.2	0.096	95	5	90	184	284	Conjugate Faulting

applied by a servo controlled stepping motor to achieve the desired confining pressure. Pore pressure (distilled water) was also applied by a servo controlled stepping motor via a 1 mm-diameter hole in the bottom endcap. The sample was taken to the target pressure and allowed to achieve pore pressure and microstructural equilibrium (ensured by monitoring the sample porosity under hydrostatic conditions) before any differential loading commenced.

The sample was then deformed in compression at an axial strain rate of 1.0×10^{-5} s^{-1}. The differential stress was taken as the axial stress minus the confining pressure. By maintaining the pore pressure constant, we could continuously monitor changes in porosity during deformation using the pore pressure intensifier. Effective pressure, P_{eff}, is calculated using a simple effective pressure law: $P_{eff} = P_c - \alpha P_p$ (where P_c and P_p are the confining pressure and pore pressure, respectively, and α is the Biot constant; Nur and Byerlee 1971). We assume that poroelastic constant α is equal to 1. A recent study by Farquharson et al. (2016) demonstrated that α for porous andesite is extremely close to 1, validating our assumption.

The output of acoustic emissions (AE) was monitored via a piezoelectric crystal fixed to the axial piston of the apparatus (Fig. 5). Similar to the observations of Vajdova et al. (2012), the AE showed negligible activity during our experiments and added no valuable information to interpret our experimental results.

3. Results

3.1. Influence of effective pressure on failure mode

To better understand the influence of effective pressure on the failure mode of the RKA, five samples of altered andesite breccia from the same core (28.14.2; Table 1) with similar porosity (average 0.096; Tables 1 and 2) were deformed under different effective pressures (from 5 to 90 MPa; see Table 2). The mechanical data show that the peak stress of the andesite samples increases with increasing effective pressure (Fig. 6a). A stress drop (strain softening) is observed immediately following the peak stress in the experiments at P_{eff} between 5 and 70 MPa (Fig. 6a), a feature characteristic to brittle failure. The post-peak stress drop is much more gradual at P_{eff} = 90 MPa (Fig. 6a). All of the porosity change curves (Fig. 6b) show that the samples undergo compaction (porosity decrease, typically interpreted as the closure of pre-existing microcracks), followed by dilation (porosity increase; a result of the nucleation and growth of new microcracks) as the samples approach macroscopic failure (peak stress). Interestingly, and despite the brittle mode of failure, the samples deformed at the highest effective pressures (70 and 90 MPa) showed net compaction at the end of the experiment (i.e. at 3% and 4.5% axial strain, respectively).

3.2. Influence of porosity on failure mode

To examine the role of porosity on failure mode, a set of seven moderately altered samples with a porosity range of 0.068–0.153 (Tables 1 and 3) were deformed at P_{eff} = 40 MPa (P_c = 60 MPa, Pp = 20 MPa; Table 3). In general, we observe that sample strength decreases with increased porosity (Fig. 7). We further highlight that the shape of the stress-strain curve changes as a function of porosity for samples with similar alteration (Fig. 8a). In particular, the magnitude of the stress drop is reduced considerably when the porosity is increased (Fig. 8a). The porosity reduction curves for these experiments (Fig. 8b) show that the samples undergo compaction followed by dilation (similar to the curves of Fig. 6b). Prior to the switch to dilatant-dominant behaviour, the high-porosity sample compacted much more than the low-porosity sample (Fig. 8b).

Although the mechanical data show that the failure mode is brittle (Fig. 8a and b), further insight can be gleaned through the macroscopic observation of the post-deformation samples. Photographs of the post-failure samples show that there is an obvious

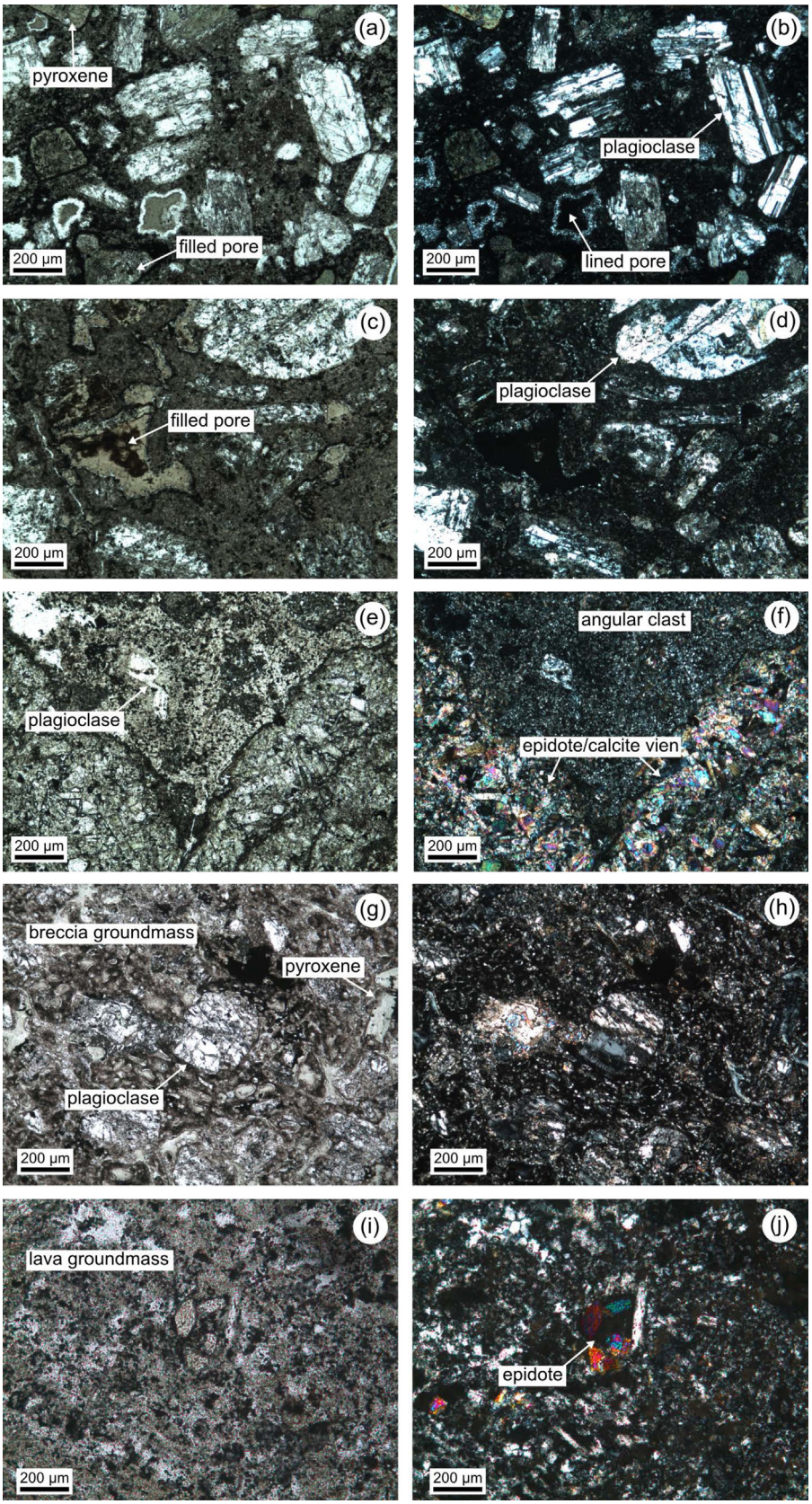

Fig. 2. Photomicrographs (left: plane polarised light; right: cross polarised light) of the key rock types used in this study. See Table 1 for sample descriptions. Sample 27L2.3.7a (panels a and b); sample 28.10.5b (c and d); sample 28.14.5 (e and f); sample 27.TJ11 (g and h); sample 29.TJ14 (i and j).

Table 3
Summary of the triaxial testing on samples of RKA with different porosities. P_c = confining pressure. P_p = pore fluid pressure. P_{eff} = effective pressure. *sample not used in the synopsis plot of Fig. 7 due to its highly altered nature (see Table 1).

Sample	P_c (MPa)	P_p (MPa)	P_{eff} (MPa)	Effective mean stress P at the peak stress (MPa)	Differential stress Q at the peak stress (MPa)	Connected Porosity	Dry bulk Density (kg/m^3)	Failure Mode
28.14.5*	60	20	40	80	122	0.140	2470.1	Shear Fracture
27.21.2b	60	20	40	99	176	0.125	2387.7	Shear Fracture
27.3.7a2	60	20	40	92	156	0.102	2501.0	Conjugate Faulting
28.11.3a	60	20	40	113	220	0.093	2482.5	Shear Fracture
28.10.5b	60	20	40	118	234	0.080	2519.6	Shear Fracture
28.11.1b2	60	20	40	107	203	0.068	2559.7	Shear Fracture
27.TJ11.1	60	20	40	103	188	0.148	2334.0	Shear Fracture
29.TJ14.2*	60	20	40	94	163	0.178	2257.0	Conjugate Faulting
27.TJ11.4	90	20	70	137	201	0.153	2325.0	Conjugate Faulting
29.TJ14.4*	90	20	70	130	180	0.178	2270.0	Conjugate Faulting

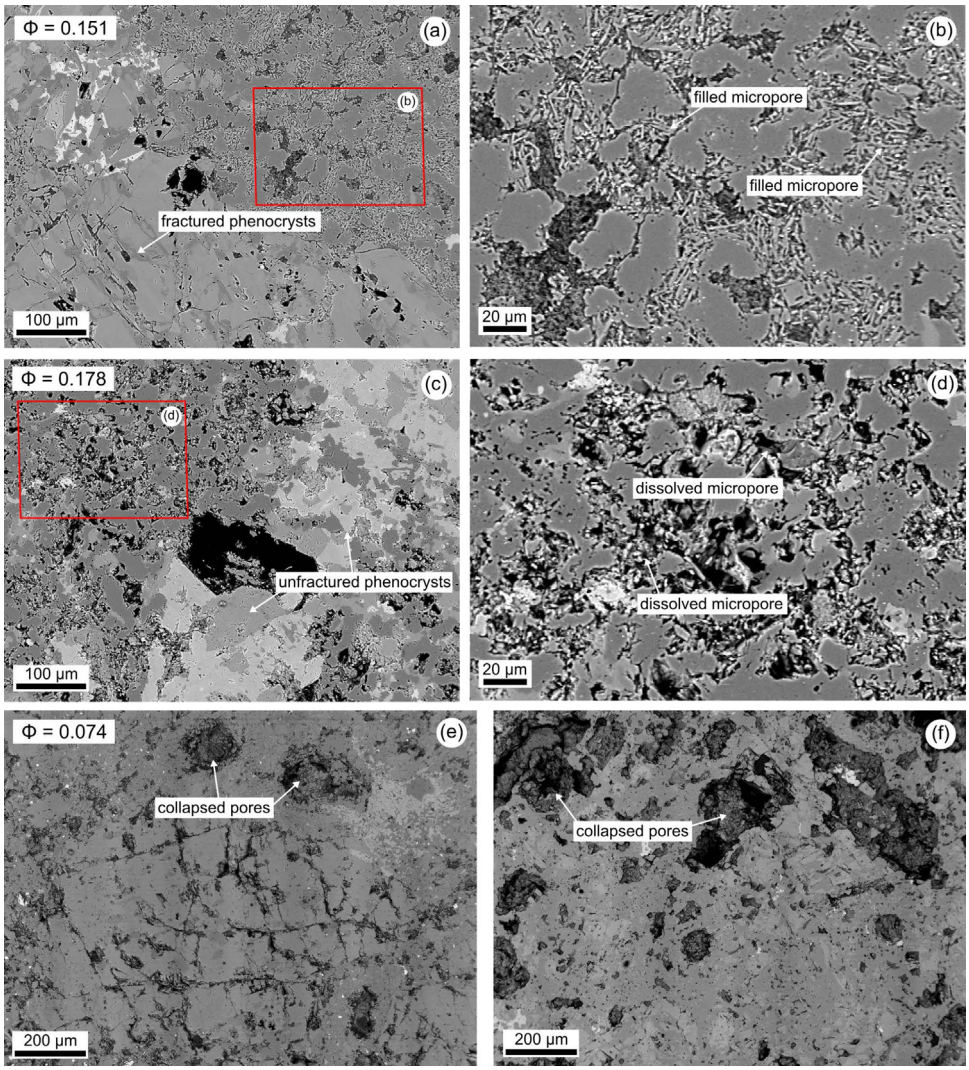

Fig. 3. Backscattered scanning electron microscope (SEM) images of intact (i.e. pre-deformation in the laboratory) RKA. Panel (a) shows the moderately altered andesite breccia containing an average porosity of 0.151 (27.TJ11). Panel (b) is a zoomed-in image of the red rectangle shown in Panel (a). Panel (c) shows the highly altered andesite lava containing an average porosity of 0.178 (29.TJ14). Panel (d) is a zoomed-in image of the red rectangle shown in Panel (c). Panels (e) and (f) show andesite containing evidence of collapsed pores (RK30.80.c12 and RK27.11.6, respectively). The important textural features are indicated on the panels. The large hole in the centre of panel (c) is assumed to be damage to the thin section rather than an actual pore. (For interpretation of the references to colour in this figure legend, the reader is referred to the web version of this article.)

shear fracture in the sample containing the lowest initial porosity (porosity = 0.068), while the sample hosting 0.102 porosity contains conjugate shear faults and exhibits slight barrelling (Fig. 8c).

3.3. *Influence of alteration on failure mode*

To demonstrate the influence of alteration on the mechanical behaviour and failure mode of the RKA, we show the mechani-

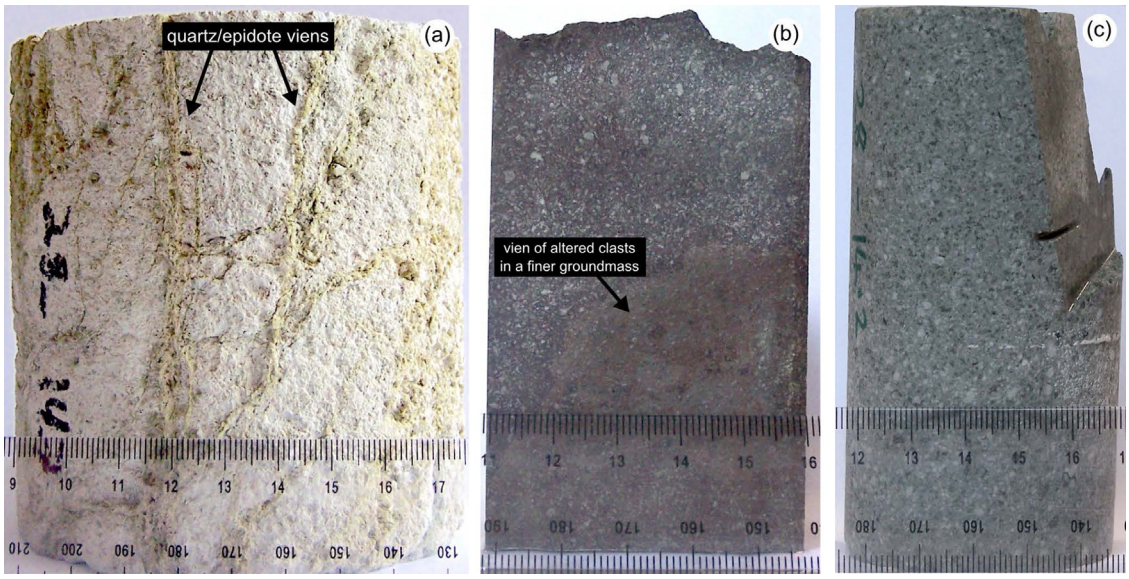

Fig. 4. Photographs of intact core of (a) sample 28.14.7 representing the breccia texture and high alteration of sample 28.14.5; (b) sample 27.TJ11 showing a moderately altered clast within a moderately altered fine grained groundmass; and (c) sample 28.14.2 showing a moderately altered lava.

cal data for two andesitic breccia samples with similar porosity (0.148 and 0.140), but different alteration intensities (moderate and high, respectively) (Fig. 9; Table 3). Both of these samples were deformed at P_{eff} = 40 MPa (P_c = 60 MPa, P_p = 20 MPa; Table 3). We find that the highly altered sample is much weaker, has a considerably shallower stress drop (Fig. 9a), and dilates much less during brittle failure (Fig. 9b). For example, while the porosity of the highly altered sample had increased by almost 0.0035 after 2.5% axial strain, the moderately altered sample had only lost a porosity of 0.0015 (Fig. 9b). We highlight that net compaction at the end of the experiment was only observed at P_{eff} = 70 and 90 MPa when the porosity was 0.096 (Fig. 6b). Macroscopic observation of the post-deformation samples showed that, while the moderately altered sample contained an obvious shear fracture, the highly altered sample contained multiple, less obvious macroscopic fractures (Fig. 9c).

To further investigate the impact of alteration on the failure mode of RKA, we show two additional experiments on highly altered lava samples (both containing a porosity of 0.178; Table 3) deformed at P_{eff} = 40 and 70 MPa (Table 3). The goal of such experiments was to understand whether high-porosity, high-alteration samples can deform in a ductile manner at elevated effective pressure. We find that the stress drops for both experiments are very shallow (Fig. 10a). In detail, the stress drop for the sample deformed at P_{eff} = 70 MPa is much lower magnitude than that for P_{eff} = 40 MPa (Fig. 10a). At P_{eff} = 40 MPa, the porosity reduction curve indicates that the sample first compacted; the sample dilated following the peak stress (Fig. 10b). The sample deformed at P_{eff} = 70 MPa did not enter a domain of dilatancy-dominance up to an axial strain of 6%, at which point the sample had lost a porosity of 0.013 (Fig. 10b). Visual inspection of the post-deformation samples indicated the presence of shear fractures in both samples (Fig. 10c). Therefore, despite the bulk compaction of the sample deformed at P_{eff} = 70 MPa, the deformation style is still classified as brittle.

3.4. Post-deformation microstructural observations

Microscopic observations allow us to understand the micromechanical processes operative during the experiments. We report here on microstructural observations of three of the samples deformed at P_{eff} = 40 MPa shown in Figs. 8 and 9. These samples were chosen for microstructural analysis on the basis of their differences in initial porosity.

SEM images of the low-porosity sample (porosity = 0.068), in which we observed a shear fracture (Fig. 8c), show the main shear fault with some associated off-fault damage (Fig. 11a and b). Away from the shear fault, the rock appears intact (i.e., the strain is localised). The intermediate-porosity sample (porosity = 0.102) shows conjugate shear fractures and an apparent barrelling of the originally straight core (Fig. 8c). Microscopically, the damage is much more diffuse than in the low-porosity sample (Fig. 11c and d); microcracks are seen within crystals, along crystal boundaries, and within the groundmass. The sample containing a porosity of 0.140 (which is also highly altered) shows multiple shear fractures and an irregularly barrelled core (Fig. 9c). We find microscopic evidence for both microcracking (sometimes orientated perpendicular to the maximum principal stress) and cataclastic pore collapse in this high-porosity and intensely altered sample (Fig. 11e and f).

4. Discussion

The results of our deformation experiments demonstrate that (1) the strength of the RKA increases with increasing confining pressure (as observed previously for rock within the brittle field, e.g. Paterson and Wong, 2005; González de Vallejo and Ferrer, 2011), (2) the strength of the RKA decreases with increasing porosity (as observed previously for volcanic materials, e.g. Heap et al., 2014a; Schaeffer et al., 2015) and, (3) the strength of the RKA decreases as the intensity of the alteration increases (as observed previously in uniaxial experiments, e.g. Pola et al., 2012, 2014; Frolova et al., 2014; Wyering et al., 2014). Importantly, our triaxial experiments have also shown that the deformation of high-porosity and/or highly altered RKA can result in a net decrease in sample porosity despite the brittle mode of failure, and that this is especially true at higher effective pressures (depths). It is important to note that all our experiments were performed at ambient temperature. Although mechanical properties such as fracture toughness may be unaffected at high-temperature (Balme et al., 2004), elevated temperatures will likely lower the strength of brittle rock due to the increased efficiency of subcritical crack growth mechanisms such as stress corrosion (Brantut et al., 2013). Further, while we emphasise that the glass-free volcanic rock is unlikely to switch from a brittle to a ductile failure mode at high temperature (low-porosity basalt remained brittle at P_{eff} = 100 MPa and 900 °C; Violay et al., 2015), we appreciate that the influence of high-temperature

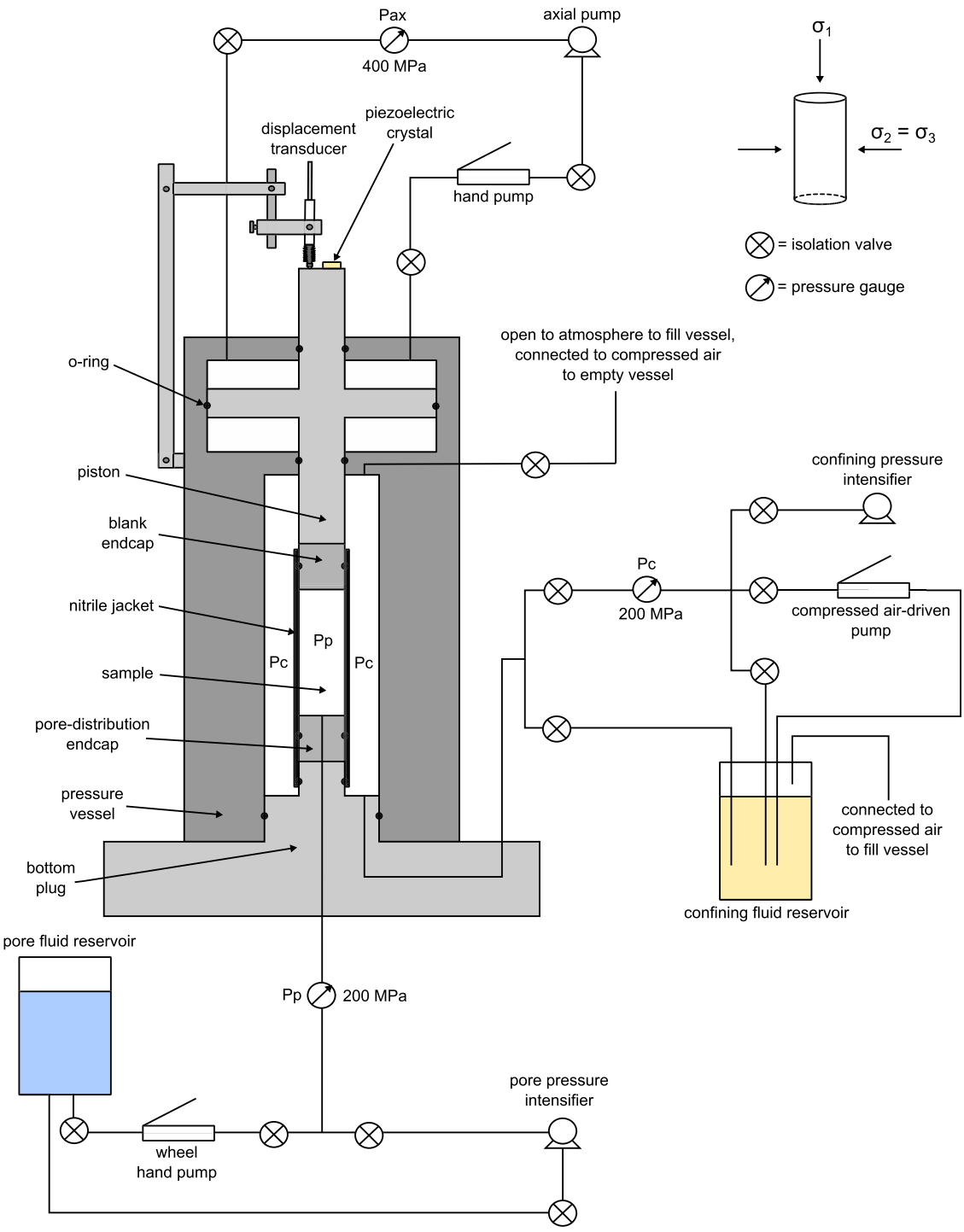

Fig. 5. Schematic diagram of the triaxial deformation apparatus at Université de Strasbourg (modified from Heap et al., 2014b). Diagram not to scale.

on highly altered volcanic rocks (containing epidote, chlorite, and calcite) is less well constrained. Future experimental campaigns will target the influence of high-temperature on the mechanical properties of the RKA.

4.1. Failure criteria for the Rotokawa Andesite

During the drilling, completion, and production/injection phases of a geothermal well, damage to the wellbore is an important consideration. Thermal (Bérard and Cornet, 2003) and mechanical stresses (Zoback et al., 1985; Zheng et al., 1989; Zoback, 2010) can potentially lead to enhanced permeability due to increased fracturing at the well wall, or well collapse when fracturing is sufficient to compromise the integrity of the wall. The experimental data presented here constrain the saturated rock strength parameters needed to analyse the risk of well damage. We constructed saturated strength criteria (Fig. 12) for the RKA of porosity 0.096 and for three other andesites, one from Whakaari volcano (New Zealand; Heap et al., 2015c) and two from Volcán de Colima (Mexico; Heap et al., 2015b). These additional materials are not only the same lithology—andesite—but the experiments were also conducted using the same methodology and equipment we

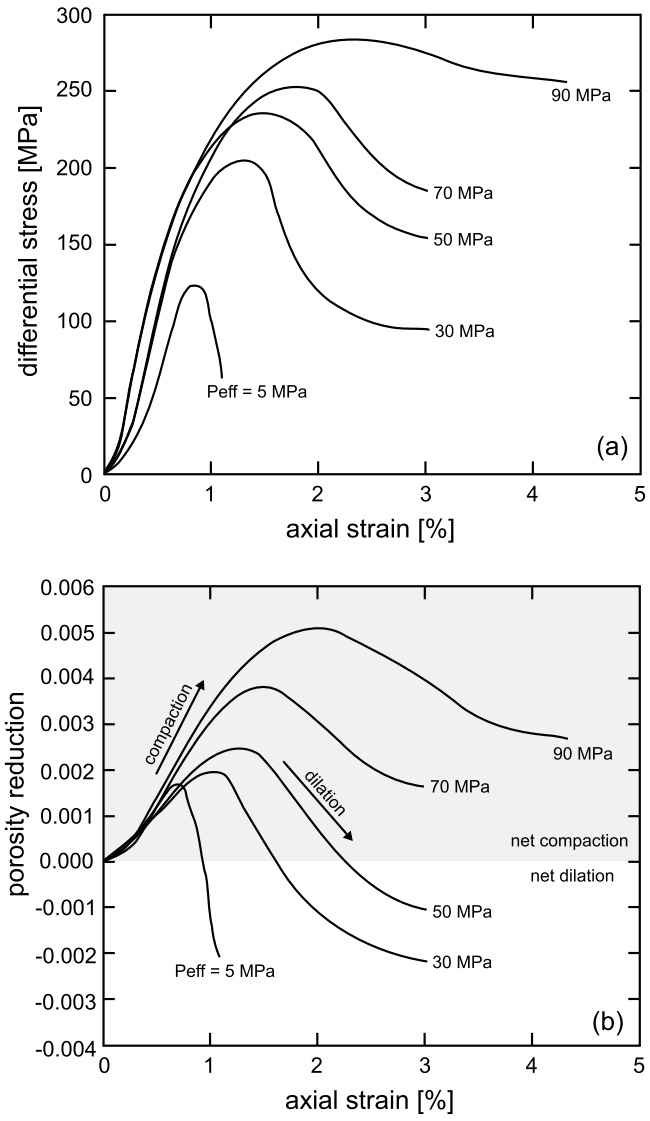

Fig. 6. Mechanical data from triaxial deformation experiments performed under different effective pressures on RKA containing an average porosity of 0.096 (Table 2). (a) Stress strain curves. The effective pressure of the experiment is indicated next to each curve. (b) Porosity reduction as a function of axial strain. The effective pressure of the experiment is indicated next to each curve. The grey zone denotes the zone of net compaction.

describe here. The saturated strength criteria are based on the Hoek-Brown failure criterion for intact rock (Hoek and Brown, 1980; Eberhardt, 2012). The Hoek-Brown failure criterion is plotted in two-dimensions using effective principal stresses. The effective major principal stress, σ'_1 = differential stress + P_{eff}, is plotted along the *y*-axis and the effective minor principal stress, $\sigma'_3 = P_{eff}$, is plotted along the *x*-axis. The failure curve for any rock is defined as $\sigma'_1 = \sigma'_3 + UCS\left(m_i \cdot \frac{\sigma'_3}{UCS} + 1\right)^{0.5}$, where UCS is the peak axial stress (σ'_1) at failure under uniaxial conditions (no confinement, $\sigma'_3 = 0$) and m_i is an empirical curve fitting parameter obtained through triaxial testing. Plotting these data in this way is useful for comparing failure criteria with *in-situ* effective pressures and changes in effective pressure due to changes in pore pressure in the reservoir or induced stresses near the wellbore. Effective pressures that fall below the strength criterion will not result in failure of the material; pressures approaching the criterion however will induce damage through new fracture initiation and/or pore collapse, depending on the material attributes. Effective pressures that fall above the strength criterion will result in failure of the intact rock.

Ductile deformation is not compatible with the Hoek-Brown failure criterion, which was constructed using P_{eff} < 0.5 UCS (Hoek and Brown, 1997; Bewick and Kaiser, 2013) for engineering purposes, such as slope stability and underground excavations, where P_{eff} tends to be much lower than UCS and failure is dominantly due to new fracture initiation (Eberhardt, 2012) and is thus brittle. The m_i factor was computed for the dataset containing the samples tested at or below P_{eff} = 0.5 UCS over which the Hoek-Brown failure criterion is considered valid. The samples tested above P_{eff} = 0.5 UCS fall below the computed criterion due to the greater proportion of compactant behaviour (pore collapse), which can initiate at lower differential stress than brittle behaviour (fracture initiation) (e.g. Wong and Baud, 2012).

Mogi's line (Mogi, 1966) represents a 3.4:1 ratio between major and minor principal stresses, and demonstrates a commonly used measure of brittle versus ductile behaviour in engineering (Bewick and Kaiser, 2013). This line is a useful visual tool for assessing stress conditions that have the potential to result in ductile behaviour. All of the failure criteria fall above Mogi's line and therefore are typically brittle rather than ductile. It is interesting to note that for the RKA of porosity 0.096, even the values beyond P_{eff} = 0.5 UCS

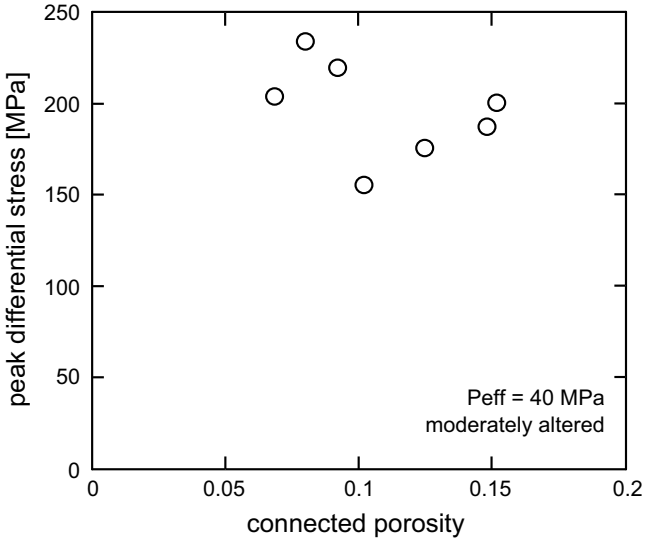

Fig. 7. Peak differential stress as a function of connected porosity for moderately altered samples of RKA deformed under an effective pressure of 40 MPa (Table 3).

fall above Mogi's line, suggesting that, while they are not valid for the Hoek-Brown failure criterion for intact rock, they also do not represent ductile failure. The peak stress for the RKA containing a porosity of 0.178 at P_{eff} = 70 MPa is 250 MPa, only slightly higher than 238 MPa, the peak stress on Mogi's line corresponding to P_{eff} = 70 MPa, showing that the failure was nearly ductile at this effective pressure (as shown in our data, Fig. 10). The data for block C8 from Volcán de Colima (porosity = 0.18) beyond P_{eff} = 0.5 UCS fall below Mogi's line, suggesting ductile behaviour achieved by cataclastic pore collapse, as discussed in Heap et al. (2015b). In addition, the RKA strength criterion is similar to that for block A5 from Volcán de Colima (porosity = ~0.1) in the effective pressure range of P_{eff} = 5–30 MPa. The strength criterion is, however, higher than the strength criteria for block C8 from Volcán de Colima and block WI20 from Whakaari volcano (porosity = 0.06). This demonstrates that, as for the type of failure observed, the strength of a rock type (such as andesite) is highly dependent on its microstructural characteristics (such as porosity and pore size and distribution; Heap et al., 2015b) and its degree of alteration, as demonstrated by Pola et al. (2012, 2014), Frolova et al. (2014), and Wyering et al. (2014, 2015).

4.2. Dilation and compaction of the Rotokawa Andesite: implications for the permeability of the Rotokawa reservoir

Our triaxial experiments on RKA show that the failure mode of low-porosity samples and/or samples at low effective pressures (i.e., shallow rock, or deeper areas of the reservoir prone to increases in pore pressure) is brittle (Figs. 6 and 8). At the end of these experiments, shear fractures had formed in the samples and the porosity of most of the samples had increased (Figs. 6b and 8b). The permeability of volcanic rocks is often a function of their porosity (Mueller et al., 2005; Wright et al., 2009; Farquharson et al., 2015), and fractures in volcanic rock are known to increase permeability (Nara et al., 2011; Heap et al., 2015b; Heap and Kennedy, 2016). It is therefore likely that the permeability of these samples had increased as a result of the imposed deformation. An increase in permeability for reservoir rock will likely increase reservoir productivity.

Our triaxial experiments also show that samples of RKA with a high-porosity and/or those deformed at high effective pressures (i.e., deep rock, or shallow areas of the reservoir prone to pore pressure reductions) suffered a net porosity reduction at the end of the experiment, despite the brittle failure mode. Although the pres-

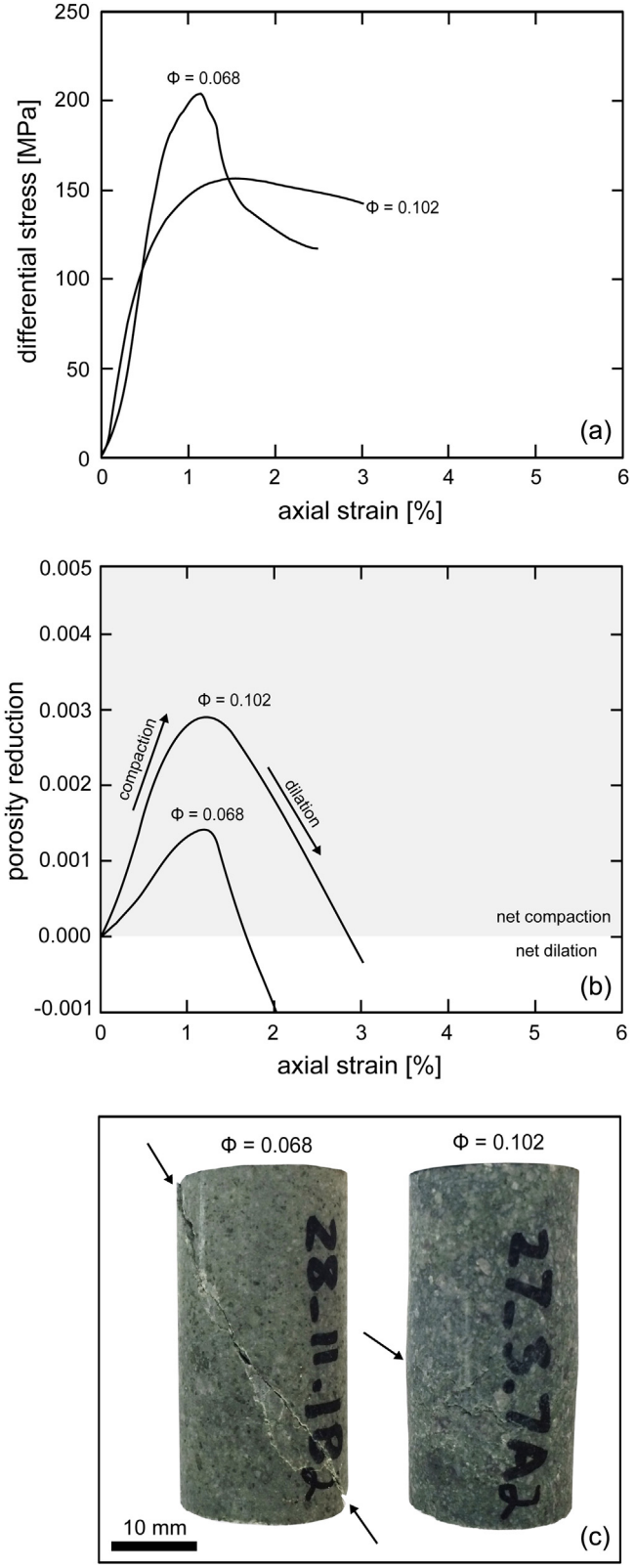

Fig. 8. Mechanical data from triaxial deformation experiments performed at an effective pressure of 40 MPa on RKA containing a porosity of 0.068 and 0.102. (a) Stress strain curves. The porosity of the sample is indicated next to the curve. (b) Porosity reduction as a function of axial strain. The porosity of the sample is indicated next to the curve. The grey zone denotes the zone of net compaction. (c) Photographs of the post-deformation samples. The arrows highlight the position of macroscopic fractures within the post-deformation samples. The sample containing a porosity of 0.068 contains a clear throughgoing shear fracture. The sample containing a porosity of 0.102 contains minor macroscopic fracturing coincident with sample barrelling.

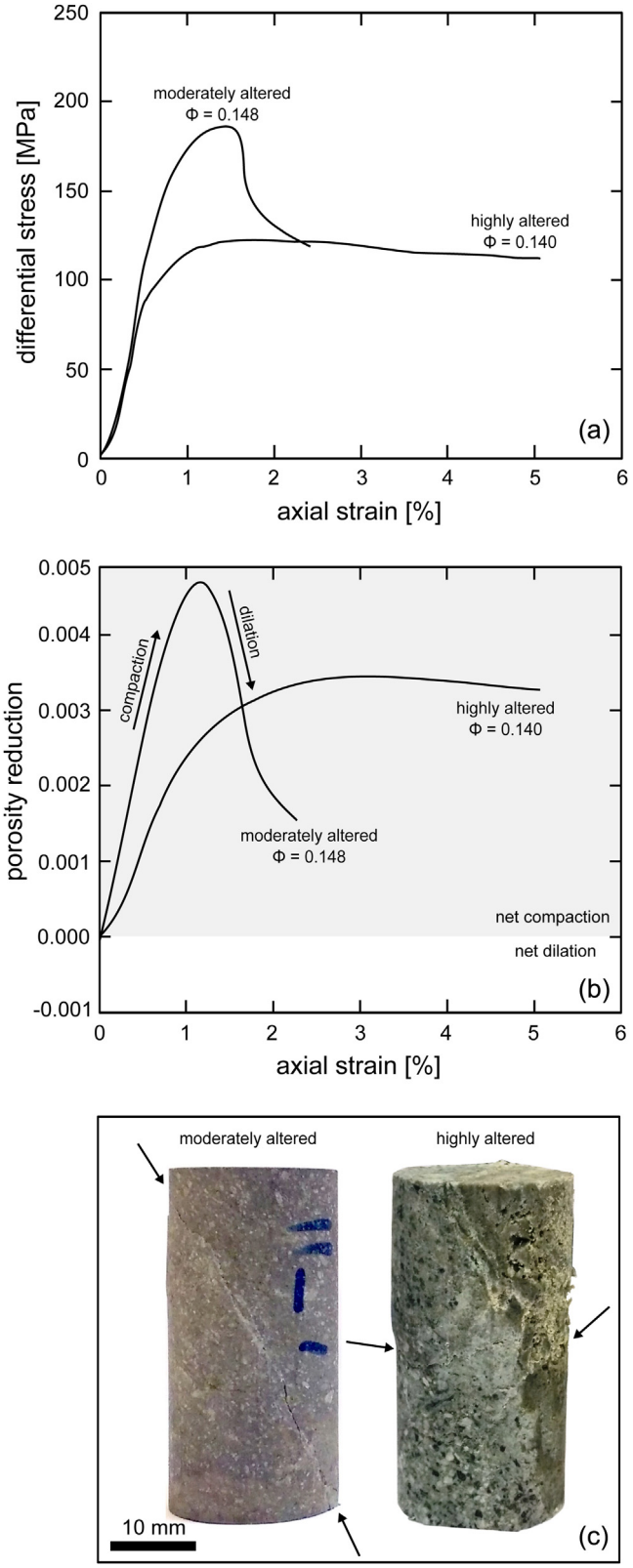

Fig. 9. Mechanical data from triaxial deformation experiments performed at an effective pressure of 40 MPa on moderately altered breccia (porosity 0.148) and highly altered breccia (porosity 0.140). (a) Stress strain curves. The porosity and alteration intensity of the sample is indicated next to the curve. (b) Porosity reduction as a function of axial strain. The porosity and alteration intensity of the sample is indicated next to the curve. The grey zone denotes the zone of net compaction. (c) Photographs of the post-deformation samples. The arrows highlight the position of macroscopic fractures within the post-deformation samples. The moderately altered sample contains a clear throughgoing shear fracture. The highly altered sample contains minor macroscopic fracturing near the middle of the sample axis.

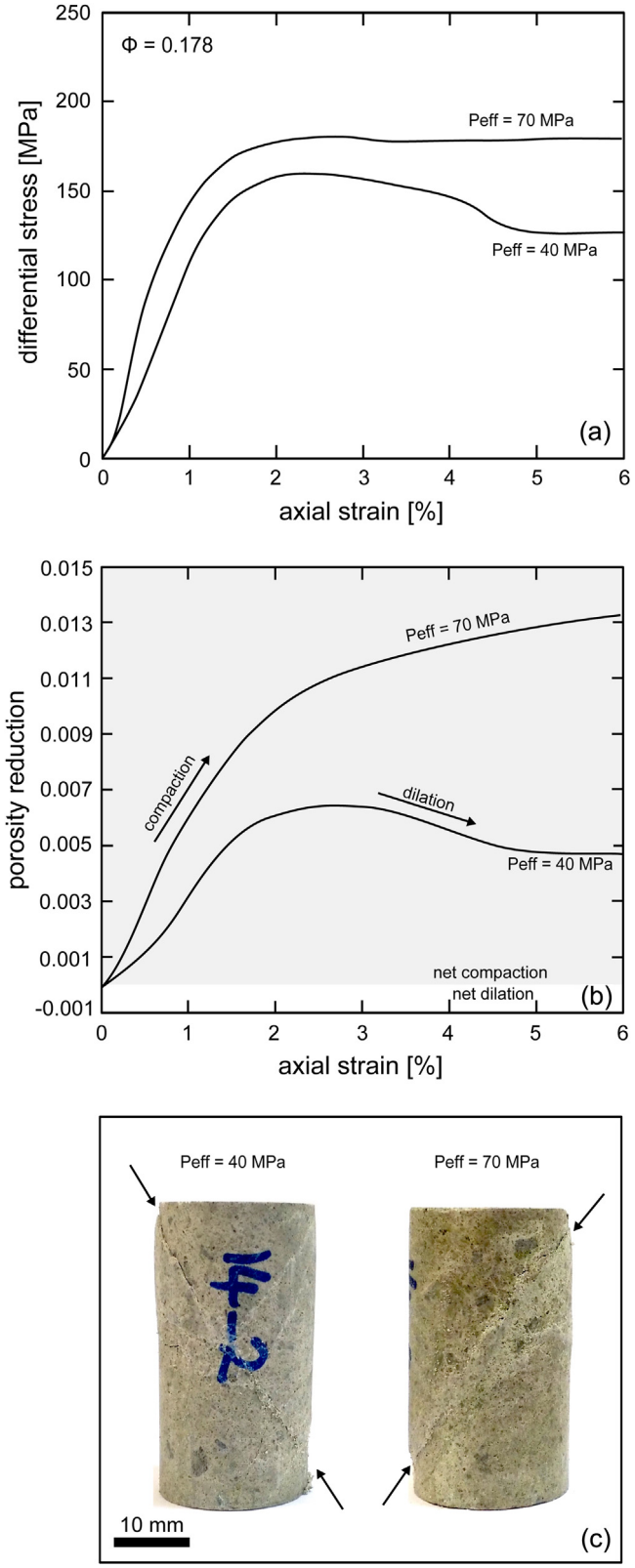

Fig. 10. Mechanical data from triaxial deformation experiments performed at an effective pressure of 40 MPa or 70 MPa on highly altered lava (average porosity = 0.178). (a) Stress strain curves. The effective pressure of the experiment is indicated next to each curve. (b) Porosity reduction as a function of axial strain. The grey zone denotes the zone of net compaction. The effective pressure of the experiment is indicated next to each curve. (c) Photographs of the post-deformation samples. The arrows highlight the position of macroscopic fractures within the post-deformation samples. Both samples contain clear throughgoing shear fractures.

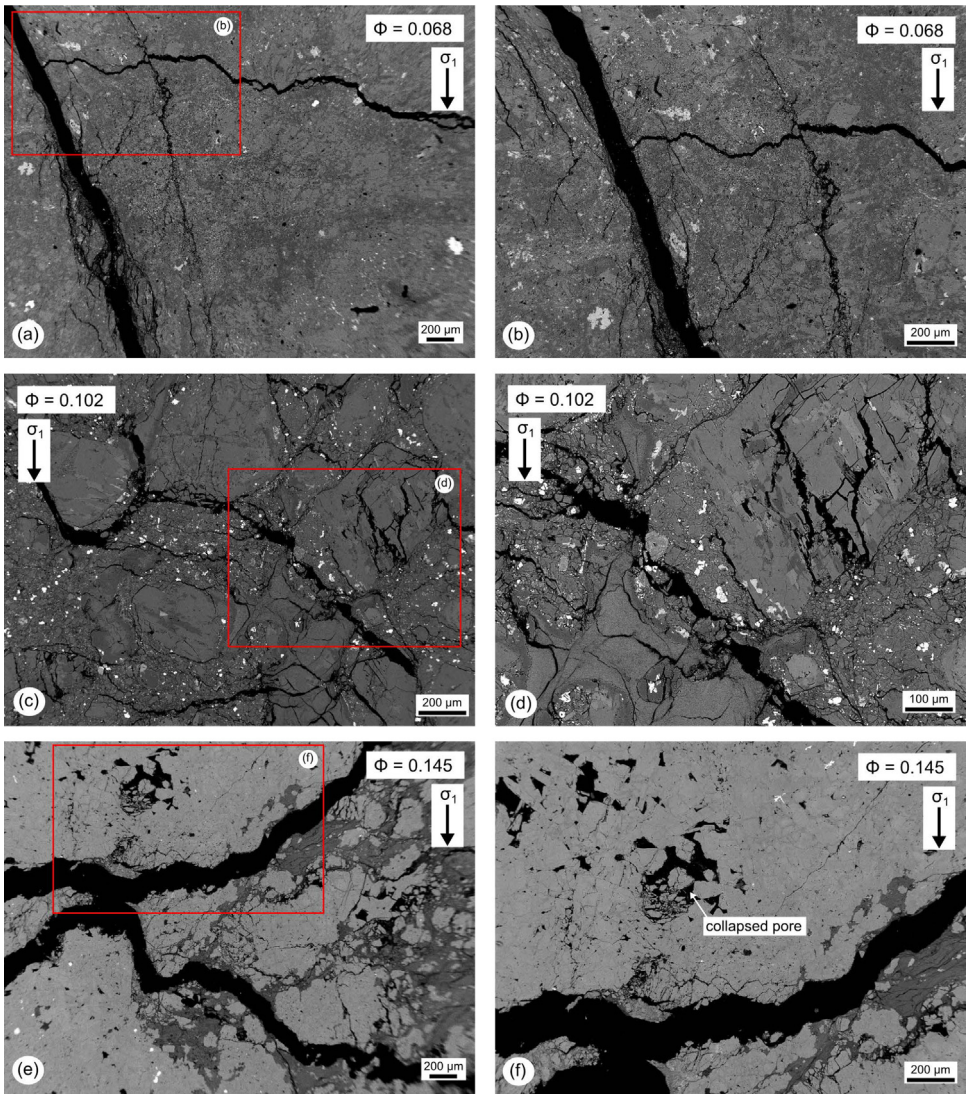

Fig. 11. Backscattered scanning electron microscope (SEM) images of post- deformation samples of RKA containing different porosities and deformed at an effective pressure of 40 MPa. Panels (a) and (b) show images of the sample of RKA containing a porosity of 0.068 (Table 3). The sample contains a throughgoing fracture with some off-fault damage. Panel (b) is a zoomed-in image of the red rectangle shown in Panel (a). Panels (c) and (d) show SEM images of the sample of RKA containing a porosity of 0.102 (Table 3). The sample contains more diffuse fracturing in both the phenocrysts and the groundmass. Panel (d) is a zoomed-in image of the red rectangle shown in Panel (c). Panels (e) and (f) show images of the sample of RKA containing a porosity of 0.140 (Table 3). The sample contains evidence of fracturing and pore collapse. Panel (f) is a zoomed-in image of the red rectangle shown in Panel (e). (For interpretation of the references to colour in this figure legend, the reader is referred to the web version of this article.)

ence of a shear fracture may locally increase the permeability, the reduction in bulk sample porosity will likely lead to a bulk reduction in permeability. For instance, Zhu and Wong (1997) show that the presence of a shear fracture in high-porosity sandstone reduces sample (i.e. equivalent) permeability. A reduction in matrix permeability, with respect to the newly-formed fracture, will likely focus the passage of fluids through the fracture. The net compaction of reservoir rock could lead to reservoir subsidence, which can be both advantageous and deleterious. For example, surface subsidence has been suggested as an exploration tool for blind reservoirs (Powell, 2011). However, subsidence can also cause damage to surface infrastructure, or to areas of significance for geothermal, cultural, or tourism purposes (Kelly, 2015; Scott et al., 2015). Our experiments on samples that preserve different intensities of propylitic alteration suggest that highly altered zones are particularly prone to stress-induced compaction (Figs. 9 and 10). The difference in mechanical behaviour between altered rocks with different alteration intensity deformed at the same effective pressure is likely linked to the weakness of some of the alteration minerals such as chlorite, calcite, and clays (Pola et al., 2012, 2014; Frolova et al., 2014; Wyering et al., 2015). Zones of intense alteration could therefore represent zones at risk of porosity and permeability reduction if, for example, pore pressure is decreased during production from the well.

The present depth of 1500–2500 m of the RKA is equivalent to pore pressures of 15–20 MPa, σ_1 of 35–60 MPa, and σ_3 of 20–30 MPa (Davidson et al., 2012); this would yield effective pressures equivalent to ~0–10 MPa. The present day mean porosity of 0.1 (Siratovich et al., 2014) implies that the dominant failure mode of the reservoir andesite is likely, therefore, to be brittle (Fig. 6), with resulting local increases in permeability. Zones of compaction and permeability decrease may be restricted to zones of intense alteration or anomalously high porosity. This recent history of brittle deformation can explain the macro-fracture dominated permeability described in the RKA (McNamara et al., 2015; Massiot et al., 2015) and the occurrence of microcracks in many samples prior to experimentation (e.g. Fig. 3). We therefore expect a signif-

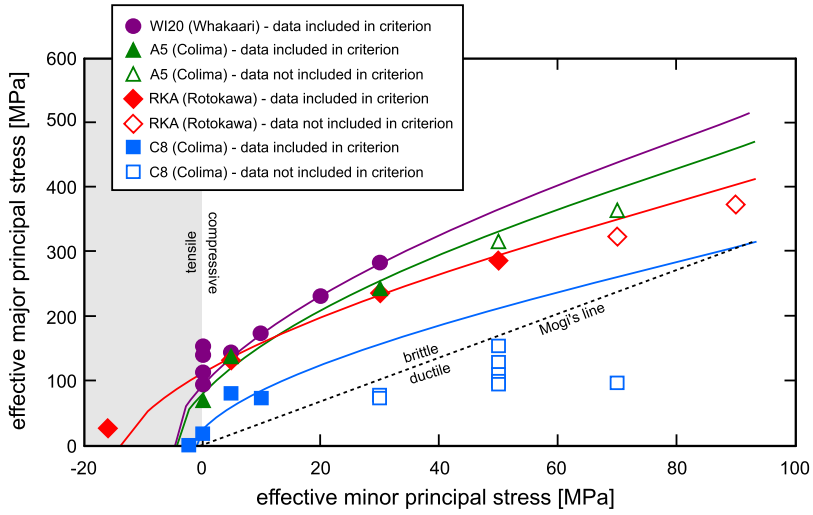

Fig. 12. Saturated failure criteria for samples of RKA containing a porosity of 0.096 compared to andesites from Volcán de Colima (Mexico) (C8 and A5; Heap et al., 2015b) and from Whakaari volcano (New Zealand) (WI21; Heap et al., 2015c). Filled symbols represent data for $\sigma_3 < 0.5$ UCS, which were used to construct the failure criteria; unfilled symbols represent data for $\sigma_3 > 0.5$ UCS, which were not used to construct the failure criteria.

icant proportion of the RKA to react in a brittle manner in response to the induced stresses during drilling, production, and extraction.

We also would like to emphasise that the nature of the porosity has likely changed dramatically during the geothermal evolution of the RKA. The RKA is more than 1.9 Ma old, based on dates from the overlying Tahorakuri Formation volcaniclastic units (Eastwood et al., 2013; Chambefort et al., 2014; McNamara et al., 2016). The RKA has therefore experienced a long period of crustal deformation and alteration. Deposition of the Tahorakuri Formation (~500 m thick) took place over at least 1 Ma, and this was followed by the emplacement of the Wairakei Ignimbrite, erupted 0.34 Ma, so that by 0.30 Ma, RKA was buried to a depth of at least 1000 m. Subsidence and deposition of more volcaniclastics and lavas have continued to bury the RKA lavas to their present depth. When originally deposited, the RKA likely had much higher porosities akin to the fresh, surface andesites measured by Heap et al. (2015b) and Farquharson et al. (2015). During burial and subsequent geothermal activity, the original pores likely collapsed (cataclastic pore collapse; see Heap et al., 2015b) or became amygdales infilled by precipitating hydrothermal alteration minerals (Fig. 3b). New pores were also formed by dissolution (e.g. Fig. 3d and Pochee, 2010; Wyering et al., 2014). Unaltered volcanic andesites of similar primary origin show a much larger range of porosity (e.g. Farquharson et al., 2015), and pores at the surface are rarely filled. Therefore, a proportion of the RKA may have historically had much higher primary porosities. We note that some samples, prior to experimentation, show some evidence of pore collapse (Fig. 3e and f) and this compaction process likely contributes to the well-documented decrease in porosity with depth in the TVZ (Wyering et al., 2015; Jones, 2016). The combined influence of burial and alteration likely resulted in a net decrease in porosity through time. This reduction in porosity over a geological timescale could explain the dominantly brittle behaviour of the present day RKA (since low-porosity rocks are likely to deform in a brittle manner, even at depth; e.g. Heap et al., 2015b).

To conclude, changes in pore pressure, alteration intensity, and porosity will all influence the mechanical behaviour, and therefore permeability development, of the RKA. We suggest the deformation mode in the RKA has varied significantly in time and space, resulting in heterogeneous porosity and permeability development as well as variations in potential deliverability of the geothermal resource.

4.3. Implications for wellbore instability

To further explore the results of our experiments, we constructed a finite element model (Phase2, Rocscience) of water-filled vertical (Fig. 13a) and deviated (Fig. 13b) wells corresponding to the RKA at 2200 m depth. The model contains the failure criterion for the RKA containing a porosity of 0.096, horizontal *in-situ* effective stresses according to Davidson et al. (2012), and production and injection are simulated using distributed forces around the excavation boundary. We find that the shear and tensile stresses surrounding the borehole wall are higher for the deviated well (Fig. 13b) than for the vertical well (Fig. 13a). This model suggests that the induced stresses are insufficiently high to initiate shear or tensile fracturing at the borehole wall for this material in a vertical well, but that minor tensile fracturing may be possible in a deviated well (Fig. 13). This is further demonstrated in the principal stress graphs of Fig. 14 that show the induced stresses during drilling (well pressure is hydrostatic), production (well pressure is equivalent to 1000 m head), and injection (well pressure is 1.5 MPa greater than hydrostatic; e.g. Davidson et al., 2012; Sherburn et al., 2015) for the vertical (Fig. 14a) and deviated (Fig. 14b) well. The principal stress graph for the vertical well shows that the stress paths for these induced stresses remain well below the failure criterion (Fig. 14a). The induced stresses around a deviated well (e.g. RK30L1 from McNamara et al., 2015) show that only minor tensile fracturing is possible during drilling for wells oriented parallel to the principal horizontal stress direction due to the higher induced mechanical tensile stresses than for a vertical well (Fig. 14b). These results are supported by observations of borehole televiewer logs of three deviated wells in the Rotokawa Geothermal Field, in which only one occurrence of borehole breakout (resulting from shearing) was observed (McNamara et al., 2015; Massiot et al., 2015). Numerous drilling-induced tensile fractures (DTIFs) were observed, but were attributed to thermal stressing (as shown experimentally by Siratovich et al., 2011, 2015a; see also Bérard and Cornet, 2003) due to the 150 °C temperature decrease during drilling, rather than mechanical stressing (McNamara et al., 2015). McNamara et al. (2015) show that the tensile stresses induced by thermal stressing inhibit shear stress-dominated borehole breakouts in the RKA. Our results show that independent of thermally-induced stress, the mechanically-induced stresses are also insufficient to create borehole breakouts. The proximity to Mogi's line of the induced stresses

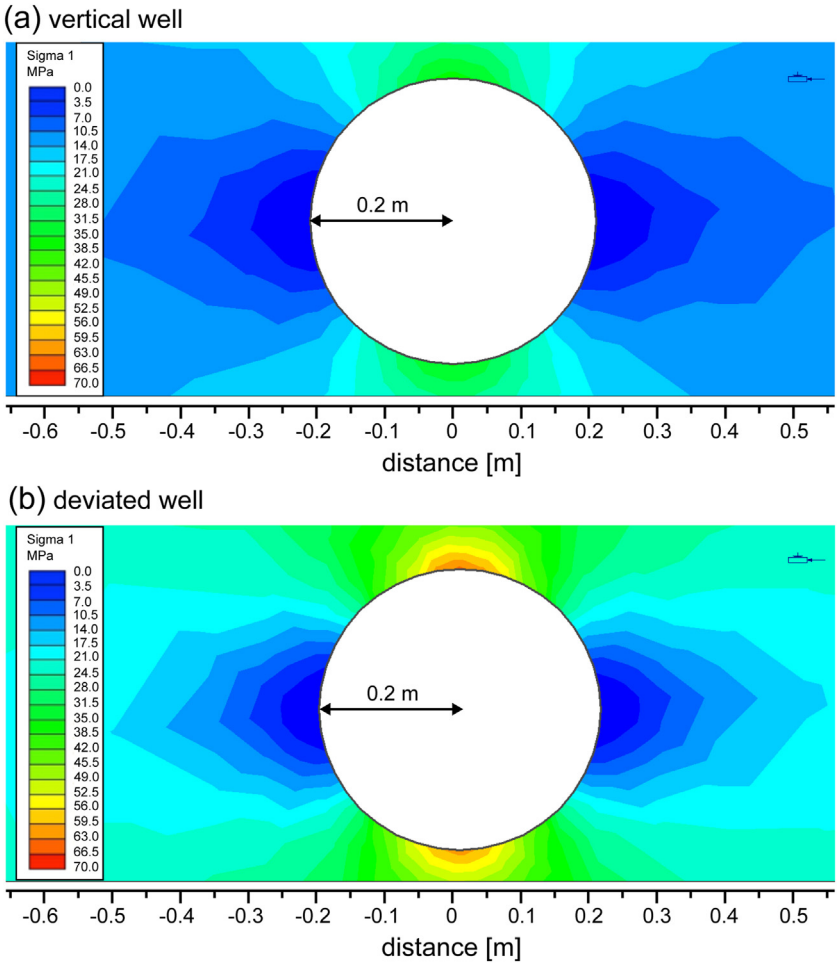

Fig. 13. Finite element model of a vertical well showing induced major principal stress around the well during drilling (well pressure is hydrostatic). No damage (in shear nor tension) was observed in this model. Field stresses are effective stresses corresponding to minimum and maximum horizontal stresses as derived by Davidson et al. (2012). This is an extensional environment where the vertical (out of plane) stress is the major principal stress.

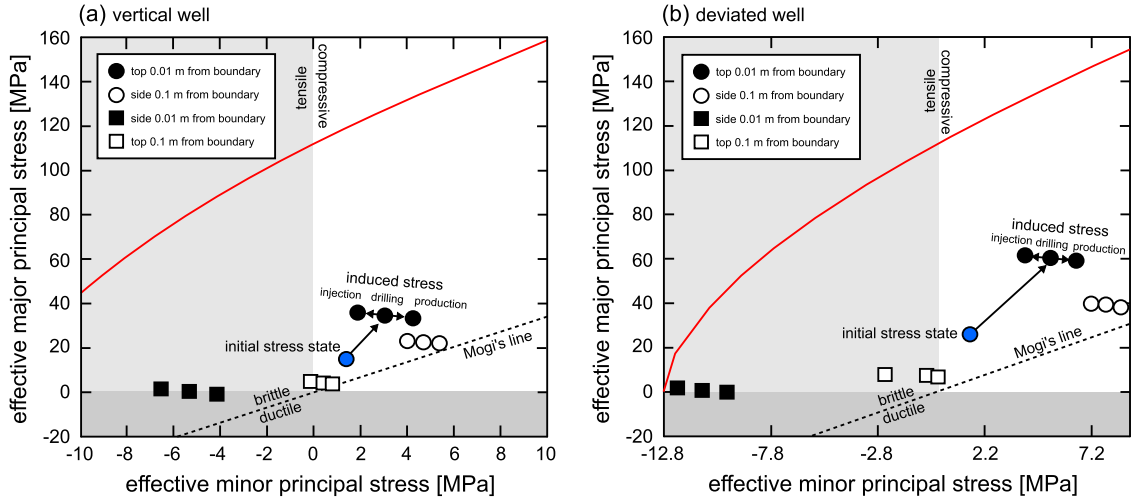

Fig. 14. Principal stress plots showing the modelled induced stresses in a vertical well (a) and a deviated well (b) at 2200 m depth compared to the failure criterion for the RKA containing a porosity of 0.096. The stress change paths for during drilling, and subsequently for reinjection or extraction, are shown for the top of the wellbore (as viewed in the model) at a distance of 0.01 m away from the excavation boundary. Similar stresses for farther from the boundary (0.1 m) and the side of the wellbore are also given, and follow similar stress change paths.

at 0.1 m from the well wall in the vertical and deviated wells during production shows that production-induced compaction may be possible for particular rock properties (for example high-porosity and/or highly altered rock) and induced stress conditions (such as those shown in Figs. 14 and 15). This is however unlikely in the Rotokawa reservoir since, as we have discussed, compaction

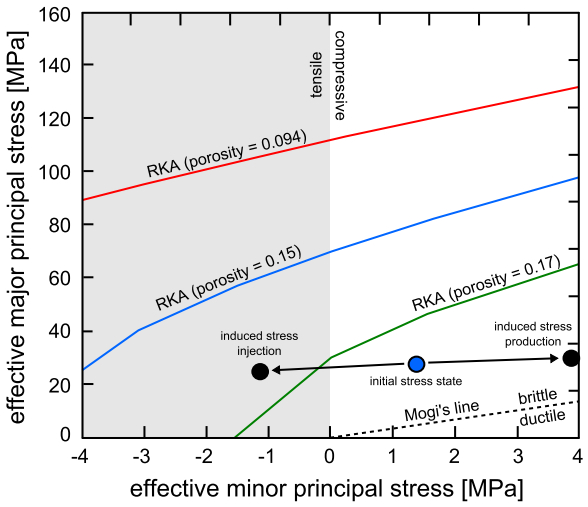

Fig. 15. Principal stress plot showing the *in-situ* stresses in a well at 2200 m depth compared to the failure criteria for the RKA samples containing a porosity of 0.096, 0.151, and 0.178. The stresses here do not include near-well induced stresses; the plot is thus valid regardless of the well orientation. The initial stress state represents the undisturbed reservoir conditions; the reinjection and extraction induced stresses represent the perturbed reservoir stresses resulting from changes in pore pressures during reservoir utilisation. Note that the samples with a porosity of 0.151 and 0.178 were not extracted from 2200 m and therefore this stress-strength combination is indicative of possible scenarios only.

(i.e. ductile behaviour) has likely already occurred through burial during the geological history of the rock, leading to a present-day failure criteria above Mogi's line (i.e. brittle).

4.4. Implications for induced seismicity

The brittle behaviour observed in our triaxial experiments implies that induced seismicity through initiation of new fractures in intact rock is possible in the RKA, and could be expected if the strength of the intact rock (for example the failure criteria given in Fig. 15) is exceeded, either by changes in differential stress or pore pressure. Most induced seismicity observed in the TVZ has been ascribed to movement on pre-existing fractures, rather than creation of new faults (Rawlinson, 2011). An examination of *in-situ* stresses, as well as stress changes induced by production and injection demonstrate that for the RKA rocks tested in this study, induced seismicity arising from fracture of intact rock during reservoir utilisation is more likely during injection than production (Fig. 15). The proximity of the production-induced stresses to Mogi's line shows that production-induced compaction may be possible in rocks with lower strength than those tested in this study, but unlikely in the RKA.

Seismicity at Rotokawa is well-documented (Sewell et al., 2012, 2013, 2015; Sherburn et al., 2015; McNamara et al., 2016) and is attributed to the thermal contraction of the reservoir rock during cold fluid injection which results in an effective pressure drop, forcing slip along faults that were already critically stressed (e.g. Davidson et al., 2012). The injection pressures used at Rotokawa are less than 1.5 MPa and are unlikely to induce a stress state that would cause failure in all but the most porous and/or most altered rocks (e.g. Fig. 15 for RKA containing a porosity of 0.178) in the large scale reservoir. However, there is a possibility that local accumulations of injected fluid may elevate pore pressure significantly enough to cause stress states favourable for deformation. This has been described by Sherburn et al. (2015) and the accepted "compartmentalisation" of the RKA reservoir (see McNamara et al., 2015) may allow development of local zones that promote both dilation and compaction in the reservoir rock purely through changes in effective pressure during injection.

5. Conclusions

Using a well-established approach to laboratory deformation we have demonstrated that the RKA, a significant geothermal reservoir, is brittle over a range of pressures relevant for the reservoir. However, despite the brittle failure mode, highly porous and/or highly altered rock, or rock deformed at high effective pressures, suffered a net reduction in porosity at the end of the experiments. By contrast, a net increase in porosity was seen for low-porosity, moderately altered rock, or rock deformed at low effective pressures. We infer therefore that brittle deformation within the reservoir may increase or decrease bulk permeability, depending on the physical attributes of the rock (porosity, alteration) and the prevalent pressure conditions (depth, pore pressure) during reservoir utilisation.

Our results also show that, under the current stress regime, seismic activity in the reservoir is likely to arise from thermal contraction and slip on already critically stressed faults rather than through elevated pore pressures, though there may be small concentrations of such seismic activity. We have further shown that borehole breakouts observed in the subsurface are unlikely to form during drilling as a result of the induced stress changes, although drilling-induced tensile fractures are likely due to thermal stresses. Production and injection are unlikely to induce compaction of the near-well reservoir; however, shearing and associated dilation is possible during injection in units with high porosity and/or high alteration intensities. Natural or anthropogenic changes to pore pressures are unlikely to result in reservoir-scale changes in porosity, although localised changes are possible due to the compartmentalisation of the Rotokawa reservoir.

This study is the first of its kind to explore the deformation behaviour of a moderately to highly altered geothermal reservoir rock under varying pressure conditions. Further study on these and similar rocks will yield further insight to the genesis, stress conditions, and mechanisms that control geothermal reservoir evolution.

Acknowledgements

Mighty River Power generously supported this work through the "Source to Surface" research grant. Tauhara North No. 2 Trust and Mighty River Power as the Rotokawa Joint Venture are thanked for the access to the samples used in this study. The authors of this study also acknowledge a Dumont d'Urville grant (number 31950RK) Hubert Curien Partnership (PHC) grant, funded and implemented by the New Zealand Ministry of Business, Innovation and Employment (MBIE), the Royal Society of New Zealand, and the Ministry of Foreign Affairs (MAEDI) and the Ministry of Higher Education and Research (MENESR) in France. M. Heap acknowledges LABEX grant ANR-11-LABX-0050_G-EAU-THERMIE-PROFONDE; this study therefore benefits from state funding managed by the Agence National de la Recherche (ANR) as part of the "Investissements d'avenir" program. We acknowledge Patrick Baud for fruitful discussions. We thank David McNamara and one anonymous reviewer for comments that helped improve this manuscript.

References

Adelinet, M., Fortin, J., Schubnel, A., Guéguen, Y., 2013. Deformation modes in an Icelandic basalt: from brittle failure to localized deformation bands. J. Volcanol. Geotherm. Res. 255, 15–25.

Allis, R., Bromley, C., Currie, S., 2009. Update on subsidence at the Wairakei-Tauhara geothermal system, New Zealand. Geothermics 38, 169–180.

Antonellini, M., Aydin, A., 1994. Effect of faulting on fluid flow in porous sandstones: petrophysical properties. Am. Assoc. Pet. Geol. Bull. 78, 277–355.
Bérard, T., Cornet, F.H., 2003. Evidence of thermally induced borehole elongation: a case study at Soultz, France. Int. J. Rock Mech. Min. Sci. 40, 1121–1140.
Balme, M.R., Rocchi, V., Jones, C., Sammonds, P., Meredith, P.G., Boon, S., 2004. Fracture toughness measurements on igneous rocks using a high-pressure, high-temperature rock fracture mechanics cell. J. Volcanol. Geotherm. Res. 132, 159–172.
Barton, C.A., Zoback, M.D., Moos, D., 1995. Fluid flow along potentially active faults in crystalline rock. Geology 23, 683–686.
Baud, P., Klein, E., Wong, T.-f., 2004. Compaction localization in porous sandstones: spatial evolution of damage and acoustic emission activity. J. Struct. Geol. 26, 603–624.
Baud, P., Vajdova, V., Wong, T.-f., 2006. Shear-enhanced compaction and strain localization: inelastic deformation and constitutive modeling of four porous sandstones. J. Geophys. Res. 111, B12401, http://dx.doi.org/10.1029/2005JB004101.
Baud, P., Vinciguerra, S., David, C., Cavallo, A., Walker, E., Reuschlé, T., 2009. Compaction and failure in high porosity carbonates: mechanical data and microstructural observations. Pure Appl. Geophys. 166, 869–898.
Baud, P., Meredith, P.G., Townend, E., 2012. Permeability evolution during triaxial compaction of an anisotropic porous sandstone. J. Geophys. Res. 117 (5), B05203, http://dx.doi.org/10.1029/2012JB009176.
Bauer, S.J., Friedman, M., Handin, J., 1981. Effects of water-saturation on strength and ductility of three igneous rocks at effective pressures to 50 MPa and temperatures to partial melting. In: Proc. 22nd U.S. Symposium Rock Mechanics, M.I.T, pp. 73–78.
Bewick, R., Kaiser, P., 2013. Discussion on an empirical failure criterion for intact rocks by Peng et al. (2013). Rock Mech. Rock Eng. 47, 817–823, http://dx.doi.org/10.1007/s00603-013-0514-4.
Bibby, H.M., Caldwell, T.G., Davey, F., Webb, T., 1995. Geophysical evidence on the structure of the Taupo Volcanic Zone and its hydrothermal circulation. J. Volcanol. Geotherm. Res. 68 (1–3), 29–58.
Brace, W.F., 1980. Permeability of crystalline and argillaceous rocks. Int. J. Rock Mech. Min. Sci. Geomech. Abstr. 17, 241–251.
Brantut, N., Heap, M.J., Meredith, P.G., Baud, P., 2013. Time-dependent cracking and brittle creep in crustal rocks: a review. J. Struct. Geol. 52, 17–43.
Browne, P.R.L., Graham, I.J., Parker, R.J., Wood, C.P., 1992. Subsurface andesite lavas and plutonic rocks in the Rotokawa and Ngatamariki geothermal systems Taupo Volcanic Zone, New Zealand. J. Volcanol. Geotherm. Res. 51, 199–215.
Caine, J.S., Evans, J.P., Forster, C.B., 1996. Fault zone architecture and permeability structure. Geology 24, 1025–1028.
Chambefort, I., Lewis, B., Wilson, C.J.N., Rae, A.J., Coutts, C., Bignall, G., Ireland, T.R., 2014. Stratigraphy and structure of the Ngatamariki geothermal system from new zircon U-Pb geochronology: implications for Taupo Volcanic Zone evolution. J. Volcanol. Geotherm. Res. 224, 51–70.
Cole, J.W., 1990. Structural control and origin of volcanism in the Taupo Volcanic Zone, New Zealand. Bull. Volcanol. 52, 445–459.
Davidson, J., Siratovich, P., Wallis, I., Gravley, D., McNamara, D., 2012. Quantifying the stress distribution at the Rotokawa Geothermal Field, New Zealand. Proceedings of the New Zealand Geothermal Workshop (November).
Eastwood, A.A., Gravley, D.M., Wilson, C.J.N., Chambefort, I., Oze, C., Cole, J.W., Ireland, T.R., 2013. U-Pb dating of subsurface pyroclastic deposits (Tahorakuri Formation) at Ngatamariki and Rotokawa Geothermal Fields. In: Proceeding 35th Geothermal Workshop, 17–20 November 2013, Rotorua, New Zealand (8pp.).
Eberhardt, E., 2012. The Hoek–Brown failure criterion. Rock Mech. Rock Eng. 45, 981–988, http://dx.doi.org/10.1007/s00603-012-0276-4.
Ellsworth, W.L., 2013. Injection induced earthquakes. Science 341, 6142, http://dx.doi.org/10.1126/science.1225942.
Evans, B., Frederich, J.T., Wong, T.-F., 1990. The brittle-ductile transition in rocks: recent experimental and theoretical progress. In: Duba, A.G., Durham, W.B., Handin, J., Wang, H.F. (Eds.), The Brittle-ductile Transition in Rocks. The Heard Volume. American Geophysical Union, Geophys Monograph 56, Washington.
Farquharson, I.J., Heap, M.J., Varley, N., Baud, P., Reuschlé, T., 2015. Permeability and porosity relationships of edifice-forming andesites: a combined field and laboratory study. J. Volcanol. Geotherm. Res. 297, 52–68.
Farquharson, I.J., Heap, M.J., Baud, P., Reuschlé, T., Varley, N., 2016. Pore pressure embrittlement in a volcanic edifice. Bull. Volcanol. 78 (6).
Frolova, J., Ladygin, V., Rychagov, S., Zukhubaya, D., 2014. Effects of hydrothermal alterations on physical and mechanical properties of rocks in the Kuril-Kamchatka island arc. Eng. Geol. 183, 80–95.
Ghassemi, A., 2012. A review of some rock mechanics issues in geothermal reservoir development. Goetechnol. Geol. Eng. 30, 647–664.
González de Vallejo, L.I., Ferrer, M., 2011. Geological Engineering. CRC Press/Balkema, Leiden, Netherlands, pp. 678.
Grant, M.A., Bixley, P.F., 2011. Geothermal Reservoir Engineering, 2nd ed. Elsevier Science Ltd., Oxford, UK.
Guéguen, Y., Palciauskas, V., 1994. Introduction to the Physics of Rocks. Princeton Univ. Press, Princeton, N.J.
Heap, M.J., Kennedy, B., 2016. Exploring the scale-dependent permeability of fractured andesite. Earth Planet. Sci. Lett. 447, 139–150, http://dx.doi.org/10.1016/j.epsl.2016.05.004.
Heap, M.J., Wadsworth, F.B., 2016. Closing an open system: pore pressure changes in permeable edifice rock at high strain rates. J. Volcanol. Geotherm. Res. 315, 40–50.
Heap, M.J., Xu, T., Chen, C.-f., 2014a. The influence of porosity and vesicle size on the brittle strength of volcanic rocks and magmas. Bull. Volcanol. 76:856, http://dx.doi.org/10.1007/s00445-014-0856-0.
Heap, M.J., Baud, P., Meredith, P.G., Vinciguerra, S., Reuschlé, T., 2014b. The permeability and elastic moduli of tuff from Campi Flegrei, Italy : implications for ground deformation modelling. Solid Earth 5, 25–44, http://dx.doi.org/10.5194/se-5-25-2014.
Heap, M.J., Brantut, N., Baud, P., Meredith, P.G., 2015a. Time-dependent compaction band formation in sandstone. J. Geophys. Res. 120, 4808–4830.
Heap, M.J., Farquharson, J., Baud, P., Lavallée, Y., Reuschlé, T., 2015b. Fracture and compaction of andesite in a volcanic edifice. Bull. Volcanol. 77:55, http://dx.doi.org/10.1007/s00445-015-0938-7.
Heap, M.J., Kennedy, B., Pernin, N., Jacquemard, L., Baud, P., Farquharson, J., Scheu, B., Lavallée, Y., Gilg, A., Letham-Brake, M., Mayer, K., Jolly, A., Reuschlé, T., Dingwell, D., 2015c. Mechanical behaviour and failure modes in the Whakaari (White Island volcano) hydrothermal system, New Zealand. J. Volcanol. Geotherm. Res. 295, 26–42, http://dx.doi.org/10.1016/j.jvolgeores.2015.02.012.
Hoek, E., Brown, E.T., 1980. Empirical strength criterion for rock masses. J. Geotechnol. Geoenviron. Eng. 106, 1013–1035.
Hoek, E., Brown, E.T., 1997. Practical estimates of rock mass strength. Int. J. Rock Mech. Min. 34, 1165–1186, http://dx.doi.org/10.1016/S1365-1609(97)80069-X.
Jones, T., 2016. Physical and Mechanical Controls of Matrix Permeability on Rocks from Rotokawa Geothermal Field, Taupo Volcanic Zone, New Zealand. MSc Thesis. University of Canterbury, New Zealand.
Keiding, M., Árnardottir, T., Jónsson, S., Decriem, J., Hooper, A., 2010. Plate boundary deformation and man-made subsidence around geothermal fields on the Reykjanes Peninsula, Iceland. J. Volcanol. Geotherm. Res. 194, 139–149.
Kelly, S., 2015. Subsidence of Cover Sequences at Kawerau Geothermal Field, Taupo Volcanic Zone, New Zealand. MSc Thesis. University of Canterbury, New Zealand.
Kennedy, L.A., Russell, J.K., Nelles, E., 2009. Origins of mount St. Helens cataclasites: experimental insights. Am. Mineral. 94, 995–1004.
Loaiza, S., Fortin, J., Schubnel, A., Gueguen, Y., Vinciguerra, S., Moreira, M., 2012. Mechanical behavior and localized failure modes in a porous basalt from the Azores. Geophys. Res. Lett. 39, L19304.
Massiot, C., McNamara, D.D., Lewis, B., 2015. Processing and analysis of high temperature geothermal acoustic borehole image logs in the Taupo Volcanic Zone, New Zealand. Geothermics 53, 190–201.
McNamara, D., Massiot, C., Lewis, B., Wallis, I., 2015. Heterogeneity of structure and stress in the Rotokawa Geothermal Field, New Zealand. J. Geophys. Res. 120, 1243–1262, http://dx.doi.org/10.1002/2014JB011480.
McNamara, D., Sewell, S., Buscarlet, E., Wallis, I.C., 2016. A review of the Rotokawa Geothermal Field, New Zealand. Geothermics 59 (Part B), 281–293, http://dx.doi.org/10.1016/j.geothermics.2015.07.007.
Menéndez, B., Zhu, W., Wong, T.-f., 1996. Micromechanics of brittle faulting and cataclastic flow in Berea sandstone. J. Struct. Geol. 18, 1–16.
Mitchell, T.M., Faulkner, D.R., 2008. Experimental measurements of permeability evolution during triaxial compression of initially intact crystalline rocks and implications for fluid flow in fault zones. J. Geophys. Res.-Solid Earth 113, http://dx.doi.org/10.1029/2008JB005588.
Mogi, K., 1966. Pressure dependence of rock strength and transition from brittle fracture to ductile flow. Bull. Earthquake Res. Inst. 44, 215–232.
Mueller, S., Melnik, O., Spieler, O., Scheu, B., Dingwell, D.B., 2005. Permeability and degassing of dome lavas undergoing rapid decompression: an experimental study. Bull. Volcanol. 67, 526–538.
Nara, Y., Meredith, P.G., Yoneda, T., Kaneko, K., 2011. Influence of macro-fractures and micro-fractures on permeability and elastic wave velocities in basalt at elevated pressure. Tectonophysics 503, 52–59.
Nur, A., Byerlee, J.D., 1971. An exact effective stress law for elastic deformation of rock with fluids. J. Geophys. Res. 76, 6414–6419.
Paterson, M.S., Wong, T.-f., 2005. Experimental Rock Deformation—The Brittle Field. Springer, New York (ISBN 978-3-540-26339-5).
Pochee, A., 2010. Mass Transfer and Hydrothermal Alteration in the Rotokawa Andesite, Rotokawa Geothermal Field, New Zealand Unpublished MSc Thesis. University of Auckland, New Zealand.
Pola, A., Crosta, G.B., Fusi, N., Barberini, V., Norini, G., 2012. Influence of alteration on physical properties of volcanic rocks. Tectonophysics 566–567, 67–86.
Pola, A., Crosta, G.B., Fusi, N., Castellanza, R., 2014. General characterization of the mechanical behaviour of different volcanic rocks with respect to alteration. Eng. Geol. 169, 1–13.
Powell, T., 2011. Natural Subsidence at the Rotokawa geothermal field and implications for permeability development. Proceedings New Zealand Geothermal Workshop 21–23 November.
Quinao, J., Sirad-Azwar, L., Clearwater, J., Hoepfinger, V., Le Brun, M., Barsdley, C., 2013. Analyses and modelling of reservoir pressure changes to interpret the Rotokawa Geothermal Field response to Nga Awa Purua Power Station operation. In: Proceedings of the 38th Workshop on Geothermal Reservoir Engineering. Stanford University, Stanford, California 11–13 February.
Rae, A.J., 2007. Rotokawa Geology and Geophysics GNS Science Consultancy Report 2010/02. GNS Science, New Zealand.
Rawling, G.C., Goodwin, L.B., Wilson, J.L., 2001. Internal architecture, permeability structure, and hydrologic significance of contrasting fault-zone types. Geology 29, 43.
Rawlinson, Z., 2011. Microseismicity Associated with Actively Exploited Geothermal Systems: Earthquake Detection and Probabilistic Location at

Rotokawa and Statistical Seismic Network Design at Kawerau. MSc Thesis. University of Victoria at Wellington, New Zealand.
Rowland, J.V., Sibson, R.H., 2004. Structural controls on hydrothermal flow in a segmented rift system, Taupo Volcanic Zone, New Zealand. Geofluids 4 (190), 89–108.
Rowland, J.V., Wilson, C.J.N., Gravley, D.M., 2010. Spatial and temporal variations in magma-assisted rifting, Taupo Volcanic Zone, New Zealand. J. Volcanol. Geotherm. Res. 122, 111–132.
Rutter, E., 1986. On the nomenclature of mode of failure transitions in rocks. Tectonophysics 122, 381–387.
Schaeffer, L.N., Kendrick, J.E., Oommen, T., Lavallée, Y., Chigna, G., 2015. Geomechanical rock properties of a basaltic volcano. Front. Earth Sci. 3 (29), http://dx.doi.org/10.3389/feart.2015.00029.
Scott, B.J., Mroczek, E.K., Burnell, J.G., Zarrouk, S.J., Seward, A., Robson, B., Graham, D.J., 2015. The Rotorua Geothermal Field: an experiment in environmental management. Geothermics 59 (Part B), 294–310.
Segall, P., Fitzgerald, S.D., 1998. A note on induced stress changes in hydrocarbon and geothermal reservoirs. Tectonophysics 289, 117–128.
Sewell, S.M., Cumming, W.B., Azwar, L., Bardsley, C., 2012. Integrated MT and natural state temperature interpretation for a conceptual model supporting reservoir numerical modelling and well targeting at the rotokawa geothermal field, New Zealand. In: Proceedings Thirty-Seventh Workshop on Geothermal Reservoir Engineering. Stanford University, Stanford, California, January 30-February 1.
Sewell, S.M., Cumming, W., Bardsley, C.J., Winick, J., Quinao, J., Wallis, I.C., Sherburn, S., Bourguignon, S., Bannister, S., 2015. Interpretation of microseismicity at the Rotokawa Geothermal Field, 2008–2015. In: Proceedings World Geothermal Congress 19-25 April 2015, Melbourne, Australia.
Sewell, S.M., Cumming, W., Bardsley, C.J., Winick, J., Quinao, J., Wallis, I.C., Sherburn, S., Bourguignon, S., Bannister, S., 2013. Interpretation of microearthquakes at the Rotokawa Geothermal Field, 2008–2012. In: 35th New Zealand Geothermal Workshop: 2013 Proceedings 17–20 November 2013, Rotorua, New Zealand.
Sherburn, S., Sewell, S.M., Bourguignon, S., Cumming, W., Bannister, S., Bardsley, C., Winick, J., Quinao, J., Wallis, I.C., 2015. Microseismicity at rotokawa geothermal field, New Zealand, 2008–2012. Geothermics 54, 23–34.
Shimada, M., 1986. Mechanism of deformation in a dry porous basalt at high pressures. Tectonophysics 121, 153–173.
Siratovich, P.A., Sass, I., Homuth, S., Bjornsson, A., 2011. Thermal stimulation of geothermal reservoirs and laboratory investigation of thermally-induced fractures. Proceeding Geothermal Resources Council Annual Meeting, 1529–1535.
Siratovich, P.A., Heap, M.J., Villeneuve, M.C., Cole, J.W., Reuschlé, T., 2014. Physical property relationships of the Rotokawa Andesite, a significant geothermal reservoir rock in the Taupo Volcanic Zone, New Zealand. Geotherm. Energy 2, 2–10, http://dx.doi.org/10.1186/s40517-014-0010-4.
Siratovich, P., Villeneuve, M., Cole, J., Kennedy, B., Bégué, F., 2015a. Saturated heating and quenching of three crustal rocks and implications for thermal stimulation of permeability in geothermal reservoirs. Int. J. Rock Mech. Min. 80, 265–280, http://dx.doi.org/10.1016/j.ijrmms.2015.09.023.
Siratovich, P.A., von Aulock, E.W., Lavallée, Y., Cole, J.W., Kennedy, B.M., Villeneuve, M.C., 2015b. Thermoelastic properties of the Rotokawa Andesite: a geothermal reservoir constraint. J. Volcanol. Geotherm. Res. 301, 1–13, http://dx.doi.org/10.1016/j.jvolgeores.2015.05.003.
Smith, R., Sammonds, P., Tuffen, H., Meredith, P.G., 2011. Evolution of the mechanics of the 2004–2008 Mt St. Helens lava dome with time and temperature. Earth Planet Sci. Lett 307, 191–200.
Townend, J., Zoback, M.D., 2000. How faulting keeps the crust strong. Geology 28, 399–402.
Vajdova, V., Baud, P., Wong, T.-F., 2004. Compaction, dilatancy and failure in porous carbonate rocks. J. Geophys. Res. 19, B05204.
Vajdova, V., Baud, P., Wu, L., Wong, T.-F., 2012. Micromechanics of inelastic compaction in two allochemical limestones. J. Struct. Geol. 43, 100–117.
Violay, M., Gilbert, B., Mainprice, D., Evans, B., Dautria, J.M., Azais, P., Pezard, P., 2012. An experimental study of the brittle-ductile transition of basalt at oceanic crust pressure and temperature conditions. J. Geophys. Res. 117, B03213.
Violay, M., Gibert, B., Mainprice, D., Burg, J.-P., 2015. Brittle versus ductile deformation as the main control of the deep fluid circulation in oceanic crust. Geophys. Res. Lett., http://dx.doi.org/10.1002/2015GL063437.
Winick, J., Powell, T., Mroczek, E., 2011. The natural-state geochemistry of the Rotokawa reservoir. In: New Zealand Geothermal Workshop 2011 Proceedings, Auckland, New Zealand.
Wong, T.-F., Baud, P., 2012. The brittle–ductile transition in rocks: a review. J. Struct. Geol. 44, 25–53.
Wong, T.-F., David, C., Zhu, W., 1997. The transition from brittle faulting to cataclastic flow in porous sandstones; mechanical deformation. J. Geophys. Res. 102, 3009–3025.
Wright, H.M.N., Cashman, K.V., Gottesfeld, E.H., Roberts, J.J., 2009. Pore structure of volcanic clasts: measurements of permeability and electrical conductivity. Earth Planet. Sci. Lett. 280, 93–104.
Wyering, L., Villeneuve, M., Wallis, I., Siratovich, P., Kennedy, B., Gravley, D., Cant, J., 2014. Mechanical and physical properties of hydrothermally altered rocks, Taupo Volcanic Zone, New Zealand. J Volcanol. Geotherm. Res. 288, 76–93, http://dx.doi.org/10.1016/j.jvolgeores.2014.10.008.
Wyering, L.D., Villeneuve, M.C., Wallis, I.C., Siratovich, P.A., Kennedy, B.M., Gravley, D.M., 2015. The development and application of the alteration strength index equation. Eng. Geol. 199, 48–61, http://dx.doi.org/10.1016/j.enggeo.2015.10.003.
Zheng, Z., Kemeny, J., Cook, N.G., 1989. Analysis of borehole breakouts. J. Geophys. Res. 94 (B6), 7171–7182.
Zhu, W., Wong, T.-f., 1997. The transition from brittle faulting to cataclastic flow: permeability evolution. J. Geophys. Res. 102 (No. B2), 3027–3041.
Zhu, W., Baud, P., Vinciguerra, S., Wong, T.-f., 2011. Micromechanics of brittle faulting and cataclastic flow in Alban Hills tuff. J. Geophys. Res. 116, B06209.
Zoback, M.D., Gorelick, S.M., 2012. Earthquake triggering and large-scale geologic storage of carbon dioxide. Proc. Natl. Acad. Sci. U. S. A. 109 (26), 10164–10168.
Zoback, M.D., Moos, D., Mastin, L., Anderson, R.N., 1985. Well bore breakouts and in situ stress. J. Geophys. Res. 90 (B7), 5523–5530.
Zoback, M.D., 2010. Reservoir Geomechanics. Cambridge University Press, Cambridge, pp. 449p.